frontiers | Frontiers in Environmental Chemistry

TYPE Original Research
PUBLISHED 23 October 2023
DOI 10.3389/fenvc.2023.1241176

OPEN ACCESS

EDITED BY
Robert Peter Mason,
University of Connecticut, United States

REVIEWED BY
John Dodson,
Chinese Academy of Sciences (CAS), China
Carl Lamborg,
University of California, Santa Cruz, United States

*CORRESPONDENCE
Jalene Nalbant,
jalene.nalbant@anu.edu.au

RECEIVED 20 June 2023
ACCEPTED 02 October 2023
PUBLISHED 23 October 2023

CITATION
Nalbant J, Schneider L, Hamilton R, Connor S, Biester H, Stuart-Williams H, Bergal-Kuvikas O, Jacobsen G and Stevenson J (2023), Fire, volcanism and climate change: the main factors controlling mercury (Hg) accumulation rates in Tropical Lake Lantoa, Sulawesi, Indonesia (~16,500–540 cal yr BP). *Front. Environ. Chem.* 4:1241176. doi: 10.3389/fenvc.2023.1241176

Fire, volcanism and climate change: the main factors controlling mercury (Hg) accumulation rates in Tropical Lake Lantoa, Sulawesi, Indonesia (~16,500–540 cal yr BP)

Jalene Nalbant[1]*, Larissa Schneider[1,2], Rebecca Hamilton[1,2], Simon Connor[1,2], Harald Biester[3], Hilary Stuart-Williams[4], Olga Bergal-Kuvikas[5], Geraldine Jacobsen[6] and Janelle Stevenson[1,2]

[1]School of Culture, History and Language, Australian National University, Canberra, ACT, Australia, [2]ARC Centre of Excellence for Australian Biodiversity and Heritage, Australian National University, Canberra, ACT, Australia, [3]Institut für Geoökologie, AG Umweltgeochemie, Technische Universität Braunschweig, Braunschweig, Germany, [4]Research School of Biology, Australian National University, Canberra, ACT, Australia, [5]Institute of Volcanology and Seismology FEB RAS, Petropavlovsk-Kamchatsky, Russia, [6]Centre for Accelerator Science, Australian Nuclear Science & Technology Organisation, Sydney, NSW, Australia

The effects of climate change on long-term mercury (Hg) cycling are still not well understood, as climate changes are usually gradual and can only be assessed using high-resolution archives. Our study site (a small, lowland tectonic lake in Sulawesi, Indonesia) provides a unique opportunity to further understanding of Hg cycling in the Southeast Asian (SEA) tropics during the transition from the Pleistocene to the Holocene, a period of significant climate variability. We present a high-resolution record of Late Glacial and Holocene Hg deposition within the sediments of tropical Lake Lantoa, Sulawesi. Using a multi-proxy framework (including pollen, charcoal, carbon:nitrogen ratio and high-resolution geochemistry records) we investigate the response of Hg accumulation rates (HgAR) in sediments to shifts in climate between ~16,488 and 538 cal BP. This period encompasses the Bølling-Allerød (BA) warming, Younger Dryas (YD) cooling and Holocene warming events, providing new insights into the effects of global climatic transitions on HgAR in SEA sediments. The Pleistocene Termination had the highest HgAR and substantial variability (μ = 11.32, 5.38–33.91 μg m^{-2} yr^{-1}), when drier conditions and high charcoal accumulation rates suggest that fire activity was the main source of Hg to the lake. The Holocene Transition was marked by a decrease in HgAR (μ = 8, 3.50–18.84 μg m^{-2} yr^{-1}) as humid conditions precluded forest burning, followed by high HgAR (μ = 11.35, 3.30–158.32 μg m^{-2} yr^{-1}) in the Early Holocene. Mercury accumulation rate in the Late Holocene (μ = 3.80, 1,67–43.65 μg m^{-2} yr^{-1}) was the lowest in the Lake Lantoa record, marked by the lowest fire events and a stable catchment. An increase in carbon:nitrogen ratios during the Late Holocene, coupled with a decrease in HgAR, suggests that the establishment of lowland forest resulted in suppressed Hg erosion/leaching. Our results demonstrate that forest fires, vegetation change and volcanism are

important drivers of Hg inputs to Lake Lantoa, a relationship which is strongly mediated by climate and lake-catchment dynamics.

KEYWORDS

volcanic mercury emissions, long-term mercury deposition, Southeast Asian mercury cycle, primary productivity and mercury accumulation, forest fire mercury emissions, effects of climate change on mercury

1 Introduction

Over the last two decades, our understanding of the biogeochemical cycling of mercury (Hg) has advanced significantly in temperate areas of the Northern Hemisphere (Lindberg et al., 2007; Obrist et al., 2018). Few studies, however, have targeted sites in the tropics (Schneider et al., 2023). This knowledge gap has meant that Hg regulatory frameworks within tropical regions have had to rely on inferences about the Hg cycle from temperate areas (Fisher and Nelson, 2020). This is problematic as there are unique processes affecting the biogeochemical cycle of Hg in the tropics, such as higher Hg uptake rates via litterfall and greater ecological heterogeneity (Lacerda et al., 1999; Wang et al., 2016; Schütze et al., 2021).

Lake systems are central to the terrestrial cycle of Hg (Parkman and Meili, 1992). They receive Hg from the atmosphere and catchment, working as natural archives that capture long-term temporal trends in Hg accumulation rates (HgAR) (Swain et al., 1992; Engstrom et al., 2007; Hermanns and Biester, 2013; Schütze et al., 2021). The HgAR is directly affected by climatic and environmental changes which play an important role in the transport of Hg from soils to lake sediments. While atmospheric deposition of Hg in lakes is a relatively straightforward process, Hg derived from the lake-catchment is dependent on complex environmental processes that need to be fully understood when reconstructing the relationship between past Hg cycling and its climatic drivers (Roulet et al., 1998; Schütze et al., 2021).

The major climatic and environmental processes that influence Hg deposition in lakes include: i) catchment erosion, ii) wet and dry deposition, iii) lake primary productivity, and iv) forest fires (Parkman and Meili, 1992; Lintern et al., 2020; Pérez-Rodríguez and Biester, 2022). Understanding these processes and how they affect HgAR over time is critical to understanding the impacts of anthropogenically-induced environmental and climatic changes on the natural Hg cycle. This is particularly relevant in the tropics, where catchment erosion is known to be intensified by high temperatures and precipitation rates, further magnifying the effects of climate and environmental changes on HgAR (Lal, 1990; Labrière et al., 2015). Furthermore, these processes are not necessarily independent, and HgAR is the net result of these dynamic processes, their proximity to the lake, and their Hg contents.

Mercury stored in soils is deposited into lakes via direct litterfall input and/or via production of dissolved organic matter (DOM), with the quantity of stored Hg dependent on the amount of Hg bound to each unit of organic matter (OM). Wet and dry Hg deposition also play an important role in regulating HgAR. Isotopic analyses indicate that 50%–80% of Hg in vegetation and soil derives from atmospheric Hg(0) uptake by plants, with the remainder from wet and aerosol deposition (Demers et al., 2013; Jiskra et al., 2015; Enrico et al., 2016; Obrist et al., 2017). This has direct implications for HgAR in tropical lakes as tropical regions have the highest global litterfall fluxes (Wang et al., 2016), resulting in higher soil Hg concentrations facilitated by the rapid breakdown of litterfall. Mercury stored in soils is deposited into lakes via direct litterfall input and/or via production of dissolved organic matter (DOM), with the quantity of stored Hg dependent on the amount of Hg bound to each unit of OM (Schütze et al., 2021).

Mercury accumulation rates in lake sediments are also mediated by primary productivity. Mercury scavenging from the water column by algae and detrital suspended particulate OM, followed by settlement and sedimentation, is recognised as an important process for Hg transfer into the hypolimnia of temperate lakes (Outridge et al., 2007; Schütze et al., 2021). Globally there is no consensus on the relationship between Hg and primary productivity in lakes, but it has been hypothesized that higher productivity results in higher HgAR (Melack and Forsberg, 2001; Schütze et al., 2021). These studies show that water column Hg scavenging by algae is the major reason for the intense Hg export to the sediments of productive lakes, making them significantly larger sedimentary sinks than oligotrophic lakes.

Forest fires are a major source of Hg deposited into lake sediments. Fires re-emit Hg sequestered in catchment vegetation and soils via volatilisation and thermal desorption (Outridge et al., 2019). Deforestation associated with forest fires promotes catchment erosion and Hg leaching into lakes (Lindberg and Stratton, 1998; Amirbahman et al., 2004), further contributing to HgAR in lake sediments. Studies have reported the coeval increase in HgAR and charcoal accumulation rates (CHAR) with peaks in charcoal counts, demonstrating the positive correlation between forest fires and HgAR (Ribeiro Guevara et al., 2010; Daga et al., 2016; Thomas et al., 2022).

Natural events (e.g., volcanic degassing, flood events, increase in catchment runoff) can also increase both direct and indirect deposition of Hg into lakes (Guédron et al., 2019). For example, a volcanic eruption emits Hg into the atmosphere, contributing to direct atmospheric Hg deposition, while volcanic ash accompanied by a release of sulphuric acid (SO_2) can trigger secondary deposition of Hg from soils via catchment erosion and Hg leaching into lakes (Guédron et al., 2019).

Southeast Asia (SEA) is critical to the global Hg cycle because it supports tropical rainforest vegetation (which facilitates Hg uptake by plants and subsequent transfer to soils and lakes) and has high regional volcanic activity (which directly contributes to atmospheric Hg emissions and subsequent deposition in terrestrial and aquatic environments). Despite the important role of tropical zones in the global Hg cycle, there are very few studies that track the long-term dynamics of Hg in relation to volcanic eruptions, landscape change and industrial activity in these areas (Pérez-Rodríguez et al., 2015; Lacerdada et al., 2017; Fadina et al., 2019; Schneider et al., 2020).

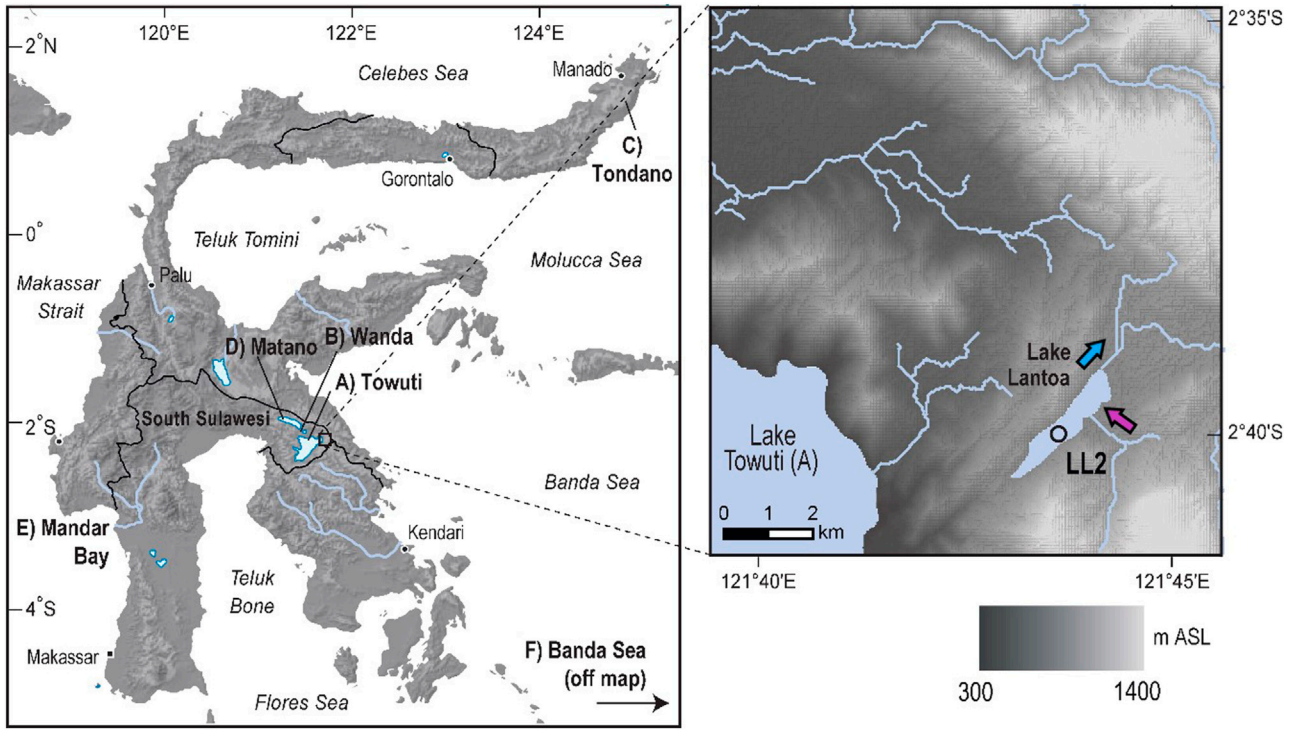

FIGURE 1
The location of the study area in South Sulawesi, Indonesia. On the right panel is a detailed figure of Lake Lantoa's catchment and its proximity to the Malili Lakes system (Lake Towuti). The coring site (LL2) is indicated by a black circle. The blue arrow on the right panel indicates the outflow of water from Lake Lantoa, and the pink arrow indicates the lake's inflow.

Long-term studies from tropical zones are crucial as they do not have the same temporal or spatial limitations as current observational studies, which typically focus on temperate regions and recent decades (Schneider et al., 2023).

We assess the impact of climate change on HgAR in tropical SEA through a long-term, multi-proxy analysis of a sediment core from a tropical lowland lake: Lake Lantoa, in Sulawesi, Indonesia. This sediment record spans ~16,500–540 cal BP, recording periods of rapid climate fluctuations from the end of the Last Glacial Maximum (Pleistocene Termination; ~18ka) into the Holocene which began ~11.7ka (Russell et al., 2016; Hamilton et al., 2019b). This provides a unique opportunity to examine the influence of highly variable climate and environmental drivers, such as vegetation and fire, on Hg cycling in the lowland tropics of SEA. In doing so we hope to expand current understanding of the relationship between lake-catchment dynamics and HgAR in tropical lake sediments, and offer insight into the effects of modern land use on Hg transport to aquatic environments.

2 Materials and methods

2.1 Study location and regional setting

Lake Lantoa (Danau Lontoa) (2.6647°S, 121.7292°E) is a low-latitude, north-east to south-east oriented lake that forms part of the much larger tectonic Malili Lakes system in South Sulawesi, Indonesia (Figure 1) (Hamilton et al., 2019b). The lake is shallow (~4 m maximum depth), small (~1.5 km^2), and sits at ~600 m above sea level (ASL). Lake Lantoa is an ideal site to study historical Hg deposition as it has a small catchment area (~5 km^2) and is fairly remote, yet it is surrounded by sub-montane vegetation on neighbouring peaks which reach up to 800 m ASL. The lake is ~29 km from the Banda Sea coast (Figure 1). Lake Lantoa receives stream inflow at the south-east and water outflows from the northern most extent of the lake (Figure 1) (Russell et al., 2016). Core LL2 was taken from the south-west of the lake, away from the inflow and outflow of water (Figure 1) (Hamilton et al., 2019b).

The Malili Lakes catchment formed approximately 1.5 Ma from a series of trans-tensional basins in response to the Matano strike-slip fault (Russell et al., 2016; Russell et al., 2020). The catchment is located within the East Sulawesi Ophiolite formation and contains ultramafic gabbros, basalts, and peridotites (Costa et al., 2015). Consequently, the catchment soils are nutrient-poor and heavy metal-rich (Van der Ent et al., 2013). Although there is archaeological evidence of human occupation in this area since 40,000 cal BP, land use prior to the development of mining in the 1970s mostly consisted of small-scale agriculture (Hope, 2001; Van Den Bergh et al., 2016). Therefore, we do not expect anthropogenic activities, such as broad-scale forest clearing, to influence our proxies. This inference is supported by pollen data published from Lake Lantoa in Hamilton et al. (2019b), which shows no obvious clearance of catchment vegetation over the past 16,500 years.

Sulawesi has a heterogenous temperature and precipitation gradient across the island, resulting in high humidity at low-

elevations and milder climate in mountainous terrain with higher altitudes (Whitten et al., 1988). As there are only 2 months where the average rainfall is <100 mm/month (September and October), Sulawesi is considered to be mildly seasonal (Walsh and Lawler, 1981).

Regional climate patterns within Sulawesi are dictated by changes in the Indo-Pacific Warm Pool (IPWP), shifts in the International Convergence Zone (ITCZ), and the El Niño Southern Oscillation (ENSO) cycle (De Deckker, 2016). Sulawesi is surrounded by the IPWP, which has a permanent sea surface temperature (SST) of >28°C (De Deckker, 2016). The IPWP directly influences the Australian-Indonesian Summer Monsoon (AISM) strength, as monsoons are generated in response to the temperature difference between the land and sea, with precipitation falling over the area with the higher surface temperature. The AISM drives a north-easterly flowing air current from the Northern Hemisphere into the Southern. Changes in AISM strength can mediate the transportation of Hg from the Northern Hemisphere into the Southern Hemisphere. This is particularly pertinent to interpreting the HgAR record in Sulawesi as it can potentially record Hg emissions from local and regional volcanism. Volcanic Hg is primarily emitted as gaseous elemental mercury (GEM) allowing it to travel long distances (Ansmann et al., 1997; Slemr and Scheel, 1998; Polvani et al., 2019).

2.2 Core location and extraction

A 600 cm long sediment core (LL2) was collected from the southern end of the lake. The core was extracted using a Geocorer in six drives, each 1 m long, as detailed in Hamilton et al. (2019b). The first metre was unconsolidated and subsampled on site at 11 cm intervals. The five basal drives were capped, sealed, and transported to the Australian National University (ANU) for storage and analysis. Cores were split lengthways, and half of the core was stored in a cool room at 4°C at the School of Culture, History and Language at the ANU, while the other half was scanned for XRF elemental analysis using an Avaatech core-scanner at the Research School of Earth Sciences at the ANU. Sediment recovery within each of the first five 1 m drives ranged from 85% to 95%. Five "no core" gaps are highlighted in the figures presented in this study for the sections with less than 100% recovery (Figure 3; Figure 4; Figure 7).

2.3 Core chronology

The original chronology for the core, based on AMS ^{14}C analysis of 10 samples (bulk sediment samples), published in Hamilton et al. (2019b) has since been refined through the radiocarbon analysis of an additional 10 bulk sediment samples from the upper portion of the core (OZY codes in Table 1). These

TABLE 1 Laboratory ID, sample type, depth and conventional ^{14}C (1σ) ages of LL2 samples used for the chronological model used in this study.

Laboratory code	Depth (cm)	Material	Reference	^{14}C date BP (±1 σ)
OZY956	3	Bulk sediment	This study	655 ± 20
OZY957	9	Bulk sediment	This study	725 ± 30
45723	16	Bulk sediment	Hamilton et al. (2019)	1138 ± 21
OZY958	26.5	Bulk sediment	This study	1375 ± 30
OZY959	33.5	Bulk sediment	This study	1770 ± 30
OZY960	39.5	Bulk sediment	This study	2425 ± 30
OZY961	44.5	Bulk sediment	This study	2635 ± 25
45724	48	Bulk sediment	Hamilton et al. (2019)	2960 ± 22
OZY962	53.5	Bulk sediment	This study	3260 ± 30
OZY963	58.5	Bulk sediment	This study	3385 ± 30
OZY964	65.5	Bulk sediment	This study	3555 ± 30
OZY965	69.5	Bulk sediment	This study	3735 ± 30
DAMS008500	70	Bulk sediment	Hamilton et al. (2019)	3858 ± 29
45725	132	Bulk sediment	Hamilton et al. (2019)	4778 ± 24
45726	232	Bulk sediment	Hamilton et al. (2019)	7627 ± 28
45727	332	Bulk sediment	Hamilton et al. (2019)	10346 ± 32
45729	432	Bulk sediment	Hamilton et al. (2019)	12098 ± 37
45730	532	Bulk sediment	Hamilton et al. (2019)	12734 ± 40
45731	580	Bulk sediment	Hamilton et al. (2019)	13471 ± 42
DAMS008501	600	Bulk sediment	Hamilton et al. (2019)	13779 ± 54

samples underwent acid-base-acid (ABA) treatment prior to conversion of the organic carbon to graphite for AMS analysis on the NEC 1 MV Vega accelerator at the Australian Nuclear Science and Technology Organisation Centre for Accelerator Science (Wilcken et al., 2015) (Table 1). A Bayesian age-depth model was produced for core sediments between 0 and 600 cm at 0.5 cm intervals using the ages returned from the twenty bulk sediment samples (Table 1). This model was produced in the package Bacon 2.5 (Blaauw and Christen, 2011) in R (Core Team, 2013), using the Southern Hemisphere calibration curve (Hogg et al., 2020) (SHCal20) and a mean accumulation rate of 20 years/cm.

The top 5 cm of the core was analysed using ^{210}Pb dating. Unsupported ^{210}Pb activities were too low for dating calculations (see Supplementary Table S3). This supports the age-model based on ^{14}C dating. For this reason, this study excludes any interpretation of the industrial era (defined here as 200 BP).

2.4 Charcoal and pollen analyses

Charcoal and palynological analysis of core sediments are reported in Hamilton et al. (2019b), the results of which are used against the updated chronological model for this study. Briefly, 31 pollen and spore samples were extracted from the core sediments for palynological analysis at approximately 20 cm intervals using standard methods (Fægri and Iverson, 1989; Caffrey and Horn, 2013). Plant microfossils were enumerated under a Zeiss AxioImager M.1 light microscope fitted with an AxioCam MRc5 camera under x400 magnification and identified using published literature from the region (Huang, 1972; Wang et al., 1995; Hamilton, et al., 2019a; Hamilton et al., 2019b; Hamilton and Stevenson, 2020). A minimum count target of 200 pollen and spores (with a minimum of 100 arboreal taxa) was set for the analysis. The pollen and spore data were classified into functional groups and habitat types through comparison with a digitised herbarium list of 28,000 specimens collected from Sulawesi and compiled by the Naturalis Biodiversity Center in Leiden, Netherlands.

Macro-charcoal (>125 µm), a proxy for local fire activity, was wet sieved contiguously from 2.5 cm^3 sediment samples (Hamilton et al., 2019b). Samples between 1 and 10 cm depth were taken from 2 cm intervals while those between 10 and 600 cm were taken from 1 cm intervals (Hamilton et al., 2019b). Macro-charcoal fragments were isolated from the subsamples following methods outlined in Stevenson and Haberle (2005). Charcoal fragments were then enumerated under a Zeiss Stemi Stereo microscope at ×20 magnification (Stevenson and Haberle, 2005).

2.5 Organic matter

The organic matter (OM) content of each sediment sub-sample was determined using weight loss-on-ignition (Wang et al., 2011) at the Palaeoworks Laboratory at the ANU. Samples were freeze dried for 48 h using the Alpha 1-2 LDplus (Martin Christ, Germany) freeze drier. Approximately 0.5 g of sediment was weighed and heated for 7 h in a muffle furnace (LABEC, model CEMLL) at 550°C. After samples cooled to room temperature, they were re-weighed to determine OM %.

2.6 Carbon and nitrogen percentage

Samples of dried sediment were weighed to the closest microgram in folded tin foil cups. These were then combusted in a Carlo-Erba EA-1110 Elemental Analyser (Carlo Erba, Milan, Italy). Gases were separated using a packed gas chromatograph (HayesSep D 80/100, Grace Davison, Australia) at room temperature and passed to a stable isotope ratio mass spectrometer (Isoprime, Micromass U.K., Manchester, U.K.). Percentages of nitrogen and carbon were calculated using the heights and areas of the mass spectrometer peaks. Carbon and nitrogen ratios (C:N) were derived by dividing %C by %N. This ratio was used to characterise the source of OM to lake sediments (i.e., allochthonous vs. autochthonous) (Riddle et al., 2022). Carbon and nitrogen percentages and C:N values are presented in Supplementary Table S1.

2.7 Mercury analysis

Mercury analysis was conducted using a Milestone Direct Mercury Analyser (DMA-80 Tri-Cell; Milestone, Bergamo, Italy) at the Palaeoworks Laboratory at the ANU. Samples were analysed using the USEPA method 7,473 (USEPA, 1998). Approximately 50 mg of each sample were weighed into nickel boats. Two blanks, two Standard Reference Materials (SRMs) and 10 replicas were run every 40 samples. Certified soil reference material NIST 2706 and SECCC WQB-1 (soil and sediment matrix) were analysed, and the results agreed well with published values (Supplementary Table S2).

Mercury accumulation rate (HgAR) in this study was defined as the deposition of Hg (concentration in ng g^{-1}) per centimetre of sediment accumulation (sedimentation rate in cm yr^{-1}). Accumulation rates (µg m^{-2} yr^{-1}) were calculated using the following equation:

$$HgAR = 10 \times SR \times DBD \times Hg$$

where SR = sedimentation rate (cm yr^{-1}); DBD = dry bulk density (g cm^{-3}); Hg = Hg concentration (ng g^{-1}).

2.8 Visual inspection for glass shards

A visual inspection for volcanic tephra was conducted in the full LL2 core. As no tephra was identified visually, sediments from the two depths with the highest Hg concentrations and HgAR (depths 220 and 241 cm) were checked for cryptotephras. These sediments were digested with hydrogen peroxide and HCl, and analysed under a scanning electron microscope (SEM) JEOL JCM-6000 at 400 X magnification and an accelerating voltage 15 kV for the identification of fine glass shards.

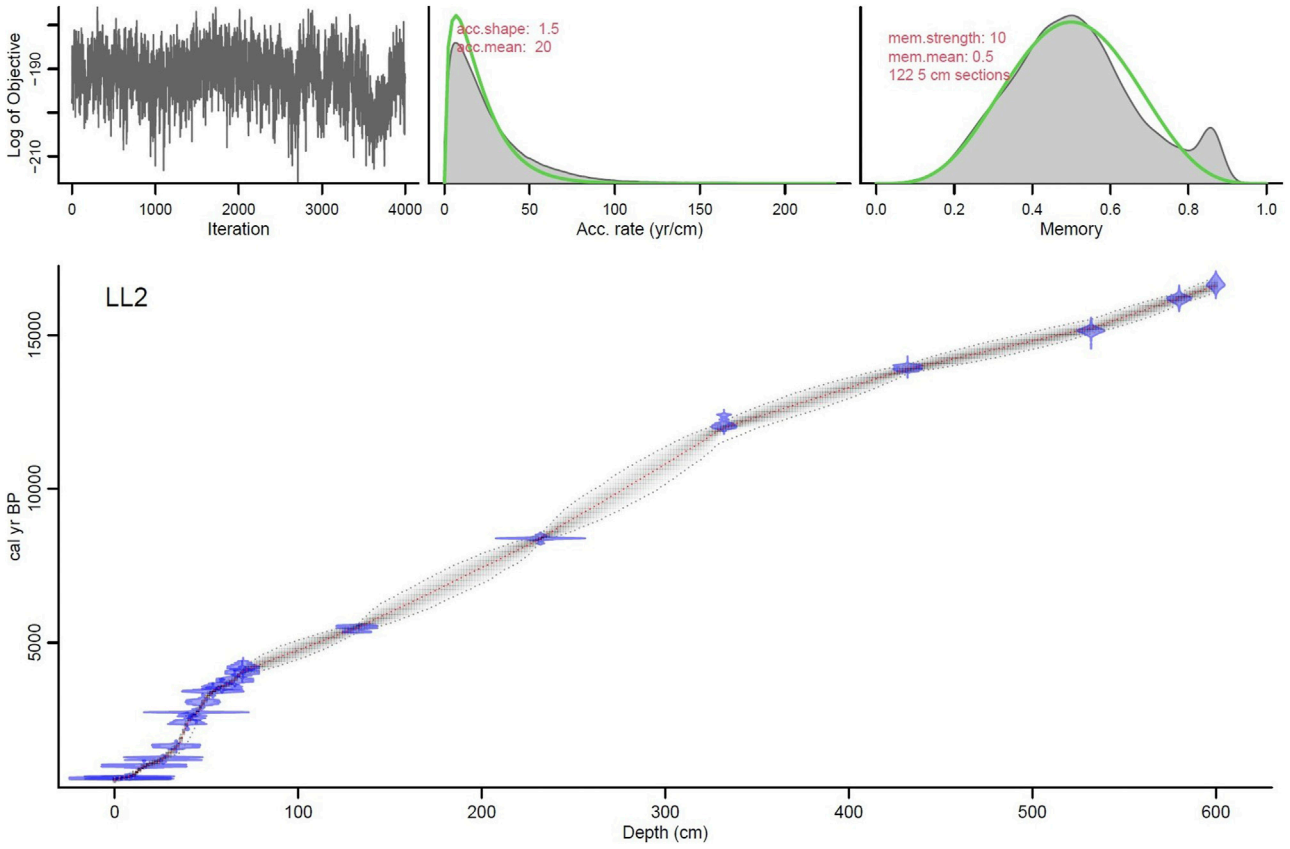

FIGURE 2
Age-depth model for Lake Lantoa sediments using R package *rbacon* 2.2 (Blaauw and Christen, 2011). The ^{14}C ages were calibrated against the Southern Hemisphere calibration (SHCal20) data set (Hogg et al., 2020). The main panel shows the age-depth model with 95% credible interval and mean as grey and red dashed line. Blue symbols indicatet the calibrated radiocarbon dates. Top panels, from left to right, show: Markov Chain Monte Carlo iterations, the accumulation rate panel with prior (green) and posterior (grey) distributions of the accumulation rate, and the memory panel (dependence of accumulation rate between neighbouring depths) showing the prior (green) and posterior (grey) distributions of the memory parameter.

2.9 X-ray fluorescence data processing and analyses

Surfaces of five core sections (100 cm–594 cm) were scanned using an Avaatech core-scanner for X-ray fluorescence (XRF) elemental analysis at the Australian National University Research School of Earth Sciences (20 s count time 10 kV voltage). The methods used to correlate and standardise these data are outlined in Hamilton et al. (2019b). In summary, this first entailed normalising each elemental variable using total count per second (cps) as the denominator, which statistical correlation determined to be a valid means of correcting for the dilution effects of water and organic material in the core sediments. Select elements that were consistently above detection limit (i.e., those that consistently returned positive count values) were then standardised using a z-score. Exceptions to this were the elements S and P which, though returning largely negative values, were included in the original study due to the interactions with redox-sensitive elements (Hamilton et al., 2019b). A running mean (centralised) was applied to the variables following normalisation (5pt for Ca, Mn, Fe, Ni, Cr; 20 pt for Al, Si, P, S, and Ti), depending on detectability and the noisiness of the dataset (Hamilton et al., 2019b). In this study any values <0 were recorded as 'below detection limits' and not included in the statistical analyses.

Lake Lantoa has a catchment characterised by ultramafic soils, composed mainly of mafic minerals (e.g., manganese [Mn], iron [Fe] and siderophilic elements such as nickel [Ni]) (Van der Ent et al., 2013). In this study, these elements (Mn, Fe, Ni) are used as a proxy for erosion ofof the Lake Lantoa catchment (Hamilton et al., 2019b).

2.10 Numerical analyses and plots

All data analyses were performed using R Statistical Software (Core Team, 2013). Stratigraphic plots were built using the R package *analogue*. Principal Component Analysis (PCA) was performed on log-transformed data using R packages *vegan*, *ggplot2* and *ggfortify*. One PCA was run with pollen, OM, C:N and charcoal data (proxies with low temporal resolution) and a second on OM, C:N charcoal and geochemical data (proxies with high resolution).

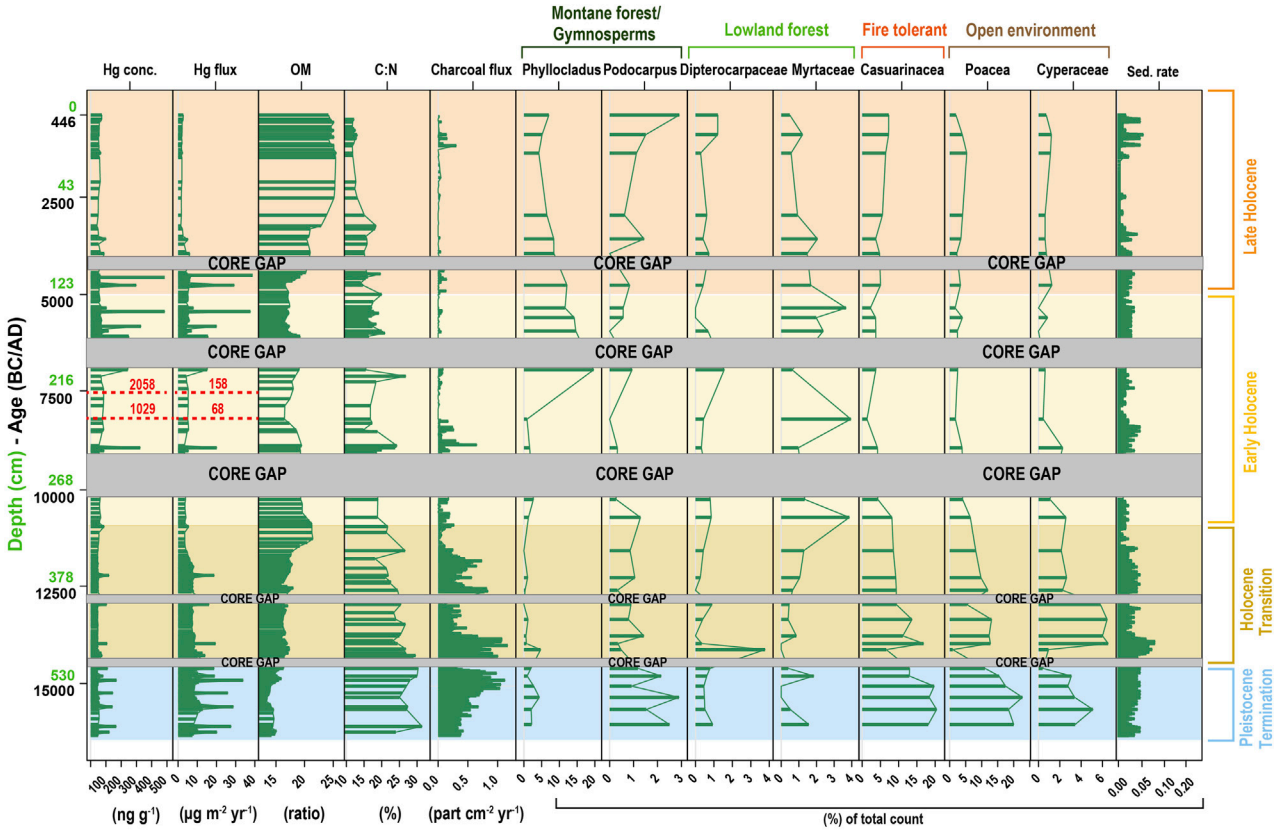

FIGURE 3
Mercury (Hg) concentrations (ng g^{-1}), mercury accumulation rate (µg m^{-2} yr^{-1}), organic matter (OM, %), carbon and nitrogen ration (C:N), charcoal flux (particle cm^{-2} yr^{-1}) and pollen data (%) for Lake Lantoa (LL2) sediment core for the last 16,477 years. The two highest peaks in Hg and HgAR (at 8,015 and 8,722 cal BP) were removed for clearer plotting of these proxies. They are represented as red dashed lines with their values and are plotted off scale.

3 Results and discussion

3.1 Core chronology, sedimentation and XRF geochemistry

The ^{14}C age-depth model for LL2 demonstrates increasing age with depth, with the smoothly varying slope indicating no, or temporally invariant, post-depositional mixing of sediments (Figure 2). The median chronological model produced for the core estimates that the age range of the sediments span 16,488–538 cal BP. The core therefore includes the Pleistocene Termination (considered to be the period between 16,488 and 14,000 cal BP in this paper), a period of significant climate variability (Russell et al., 2016).

The base of the core (594 cm) generated a mean radiocarbon age of 16,488 (16,259–16,736) cal BP and the top sample (0 cm) generated a mean radiocarbon age of 538 (446–607) cal BP. The very top part of the mud-water interface core was lost during extrusion.

The updated chronology produced for the core sediments estimates that the five core gaps capture the time periods between 14,843–14,516 cal BP, 13,293–12,967 cal BP, 10,835–9,547 cal BP, 7,475–6,552 cal BP, and 4,837–4,219 cal BP.

The age-depth model suggests a mean sedimentation rate of approximately 3 mm/yr and steadily decreases up-core. Sediments between 594 and 345 cm depth (modelled at 16,488 to 12,247 cal BP) show the fastest sedimentation rate of 4 mm/yr, slowing to 3 mm/yr between 345 and 259 cm depth (modelled at 12,247–9,378 cal BP) before slowing again to 2 mm/yr between 259 and 0 cm depth (modelled at 9,378–538 cal BP).

The XRF geochemistry results are discussed in (Hamilton et al., 2019b) and the reader is referred to the original publication for more detail. To summarise, the Lake Lantoa XRF record demonstrates that sulphur (S), manganese (Mn) and nickel (Ni) are better indicators of detrital input than some traditional elements in the Lake Lantoa catchment (Hamilton et al., 2019b). Typically, studies using XRF core scanning data report that increases in aluminium (Al), silicon (Si), calcium (Ca), titanium (Ti), magnesium (Mg), manganese (Mn) and iron (Fe) are good proxies for an increase in detrital input to lake sediments (Davies et al., 2015). As outlined in Hamilton et al. (2019b), this discrepancy is driven by the ultramafic local geology and soil type in the Lake Lantoa catchment.

3.2 Environmental and ecological changes

The results for the new proxies analysed as part of this study (Hg concentration, HgAR, organic matter, CHAR and C:N ratios) are presented in Supplementary Table S4. The cross-comparative pollen

TABLE 2 Mean of quantitative proxies (min–max) per period for core LL2.

Quantitative proxies	Pleistocene Termination (16,477–14,000 cal BP)	Holocene Transition (14,000–11,700 cal BP)	Early Holocene (11,700–5,000 cal BP)	Late Holocene (5,000–538 cal BP)
Mercury concentration (ng g^{-1})	61 (28.92–169.78)	50 (29.40–120.43)	164 (49.36–2558.59)	72 (41.13–604.70)
Mercury accumulation rate (μg m^{-2} yr^{-1})	11 (5.38–33.92)	8 (3.50–18.84)	11 (3.30–158.32)	4 (1.67–43.65)
Charcoal flux (particle cm^{-2} yr^{-1})	0.59 (0.12–1.31)	0.34 (0.01–1.00)	0.05 (0.00–0.63)	0.02 (0.00–0.24)
C:N ratio	27 (23.20–31.40)	23 (18.10–26.70)	18 (14.10–26.80)	14 (11.70–19.70)
Organic matter (%)	16 (13.36–17.39)	17 (15.66–21.45)	18 (16.48–21.28)	23 (18.36–25.53)

and XRF count data are included in the publication where these data were originally produced and interpreted (Hamilton et al., 2019b).

The Pleistocene Termination was a period characterised by relatively high local fire activity, indicated by elevated charcoal counts with a more seasonal, drier, cooler climate than the Holocene (Figure 3). In the lowlands these conditions supported a seasonal, more fire-tolerant lowland forest (e.g., Casuarinaceae) and open savanna taxa (e.g., Poaceae and Cyperceae), limiting the range of moisture-demanding, fire-exclusionary lowland and montane forest taxa (e.g., *Phyllocladus* and Dipterocarpaceae, as described in Hamilton et al., 2019b) (Figure 3). The pollen data indicate that the *Podocarpus* forest likely grew in cool, high elevation zones (Hamilton et al., 2019b).

The high C:N ratios (μ = 27, 1σ = 2.46) for the Pleistocene Termination indicate that there was significant contribution of catchment-derived organic matter (OM) to the lake (Figure 3). Typically autochthonous (within lake production) OM, like algae and phytoplankton, have more nitrogen (N) than terrestrial OM, returning a C:N ratio between 4 and 10 (Devesa-Rey and Barral, 2012). Conversely, allochthonous (catchment-derived) OM tend to be nitrogen-poor (dependent on lignin and cellulose structure) and are characterised by C:N ratios of >20 (Devesa-Rey and Barral, 2012). The C:N ratio decreases from the Pleistocene Termination to the Holocene Transition (μ = 27, 1σ = 2.46, to μ = 23, 1σ = 2.58, respectively), indicating a slight decrease in catchment-derived OM in the sediments (Figure 3 and Table 2).

Vegetation change from the Pleistocene Termination to the Holocene Transition (between 14,000 and 11,000 cal BP) suggests a gradual increase in humidity at the site (Hamilton et al., 2019b). Montane forest taxa (e.g., *Podocarpus*) and lowland ultramafic forest angiosperms (e.g., Dipterocarpaceae and Myrtaceae) gradually increase in this period, concurrent with a decline in grasses and sedges (e.g., Poaceae and Cyperaceae) and reduction in fire activity (e.g., Casuarinaceae and CHAR, as described in Hamilton et al., 2019b) (Figure 3). This climate shift is concurrent with the Bølling-Allerød, which was likely a gradual warming event in Southeast Asia (SEA) (Russell et al., 2014; Wicaksono et al., 2015; Hamilton et al., 2019b) and as a more abrupt warming event in the mid-high latitudes of the Northern Hemisphere (Benson et al., 1997).

The Early Holocene (~11,700 to 5,000 cal BP) climate of the region appears to have been relatively warm and wet (Figure 3). The pollen record indicates a shift from a more seasonal forest during the Pleistocene Termination to an everwet, fire-precluding lowland forest which persists to the top of the record (Figure 3) (Hamilton et al., 2019b). The Late Holocene (interpreted here as the period after ~5,000 BP) is characterised by a more stable climate and local catchment, with an increase in primary productivity, as indicated by the lowest C:N ratios (μ = 14, 1σ = 2.17) in the core (Figure 3 and Table 2). A slight increase in secondary/seasonal taxa (e.g., Casuarinaceae) in the pollen records after 5,000 cal BP suggests either a slight increase in aridity or heightened human activity in the catchment (Hamilton et al., 2019b).

3.3 Mercury concentration and accumulation rates

Mercury concentrations and HgAR varied along the core from 29 to 2,558 ng g^{-1} (1σ = 201.09) and 1.67–158 μg m^{-2} yr^{-1} (1σ = 13.30), respectively. For a better visualisation of the data and clearer recognition of patterns and trends for the full core, the two largest HgAR peaks (158 and 68 μg m^{-2} yr^{-1} at ~ 8,015 and ~8,722 cal BP, respectively) were plotted out of scale in Figure 3, Figure 4 and Figure 7. No XRF data is available for the top section of the core (0–100 cm) as its unconsolidated nature required this section to be sliced in the field. The contribution of catchment input in Hg concentration and accumulation rates in Lake Lantoa can be tracked through C:N ratios, which varied between 11.70 and 31.40 (1σ = 5.24) (Figure 4 and Table 2).

3.3.1 Pleistocene Termination (~16,488 to 14,000 cal BP; 594–439 cm)

The abundance of open environment pollen taxa (Poaceae and Cyperceae), limited moisture-demanding tropical taxa (Myrtaceae and *Phyllocladus*) and high charcoal counts (Figure 3) indicate that this period was characterised by a drier, more seasonal environment with relatively more forest fires (Hamilton et al., 2019b). Our results agree with global (Power et al., 2008) and regional charcoal records (Figure 3) which suggest that fire increased in the tropics during the Pleistocene Termination. This is supported by the XRF data (Figure 4) which indicate that the Lake Lantoa catchment received relatively less precipitation during the Pleistocene Termination (Hamilton et al., 2019b). These data in conjunction with the coeval increase in CHAR and HgAR demonstrate that forest fires were the main drivers of high HgAR in Lake Lantoa during the Pleistocene Termination.

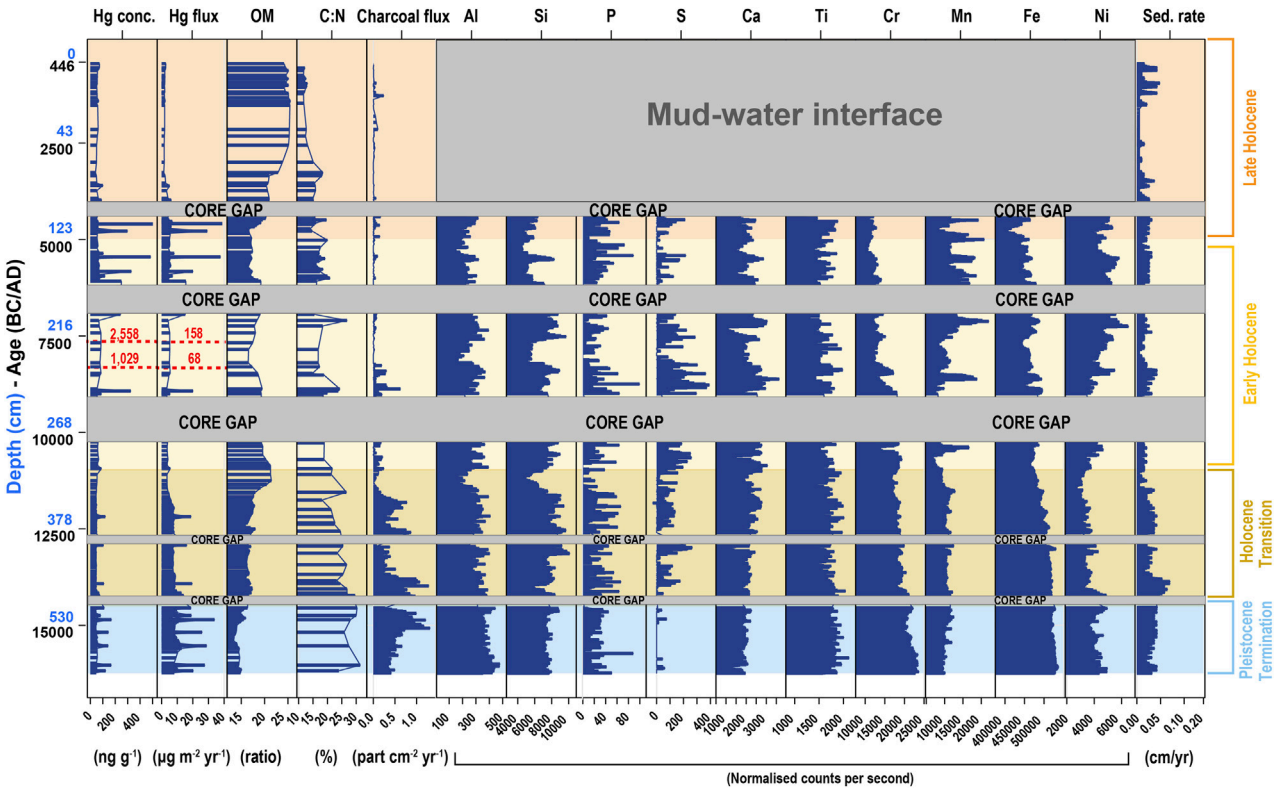

FIGURE 4
Mercury (Hg) concentrations (ng g^{-1}), mercury accumulation rate (µg m^{-2} yr^{-1}), organic matter (OM, %), charcoal flux (particle cm^{-2} yr^{-1}) and XRF data (counts per second) for Lake Lantoa (LL2) sediment core for the last 16,488 years. The two highest peaks in Hg and HgAR (at 8,015 and 8,722 cal BP) were removed to allow better visualisation of Hg concentration and accumulation rate along the core. They are represented as red dashed lines with their values and are plotted off scale.

In the Lake Lantoa record, more open, seasonal forests with grass in the understorey co-occur with higher variability in HgAR (Figure 3). This vegetation type, which burns and potentially exposes soils, may facilitate soil erosion (decreased catchment stability). Catchment stability directly impacts the type of OM (i.e., allochthonous vs. autochthonous) that is deposited into the lake, with an increase in allochthonous OM indicating an increase in catchment input to lake sediments. During the Pleistocene Termination, the C:N ratio values (μ = 27, 1σ = 2.46) indicate that Lake Lantoa received the most catchment-derived OM for the entire record (Figure 3 and Table 2). Furthermore, the sedimentation rate is the highest during the Pleistocene Termination (Figure 2), suggesting that this was a period characterised by an unstable catchment. Together these data indicate that the vegetation type in the Lake Lantoa catchment mediates the role of catchment soils as long-term Hg sinks.

The increased catchment input to Lake Lantoa sediments, as inferred from C:N ratios, OM and sedimentation rates, suggests that the Hg record is a mixture of atmospheric Hg directly deposited into the lake and secondary deposition of Hg from the catchment soils. Low manganese (Mn) and nickel (Ni) counts (Figure 4) indicate that overall there was little catchment erosion (i.e., few high precipitation/flood events) during the Pleistocene Termination (Hamilton et al., 2019b), likely due to the dry climate limiting precipitation in the Lake Lantoa catchment. The pollen, CHAR, XRF and C:N ratio data indicate that during the Pleistocene Termination the majority of the Hg in the Lake Lantoa sediments was derived from the catchment and deposited via dry or aeolian deposition. The relationship between CHAR and HgAR in the Pleistocene Termination appears to mediate aeolian deposition of Hg, with high intensity fire events associated with an increase in HgAR and C:N ratios (Figure 3). The contribution of volcanic emissions to this period is unlikely given the low sulphur (S) counts for this period (Figure 4). Therefore, dry or aeolian deposition and forest fires are the primary drivers of HgAR in Lake Lantoa sediments during the Pleistocene Termination.

3.3.2 Transition to the Holocene (~14,000 to 11,700 cal BP; 439–310 cm)

For the period between 14,000 and 11,700 cal BP, the pollen data suggest an increase in humidity, with a vegetation shift to a closed, ultramafic, lowland rainforest (Hamilton et al., 2019b) (Figure 3). While the pollen data potentially indicate an abrupt shift at ~14,000 cal BP, this is not picked up by geochemical interpretations of lake level fluctuations (Hamilton et al., 2019b) or other records from the Southern Hemisphere tropics (Colinvaux et al., 1996; Anhuf et al., 2006; Chabangborn et al., 2014; Russell et al., 2014; Partin et al., 2015; Renssen et al., 2018; Turu et al., 2021).

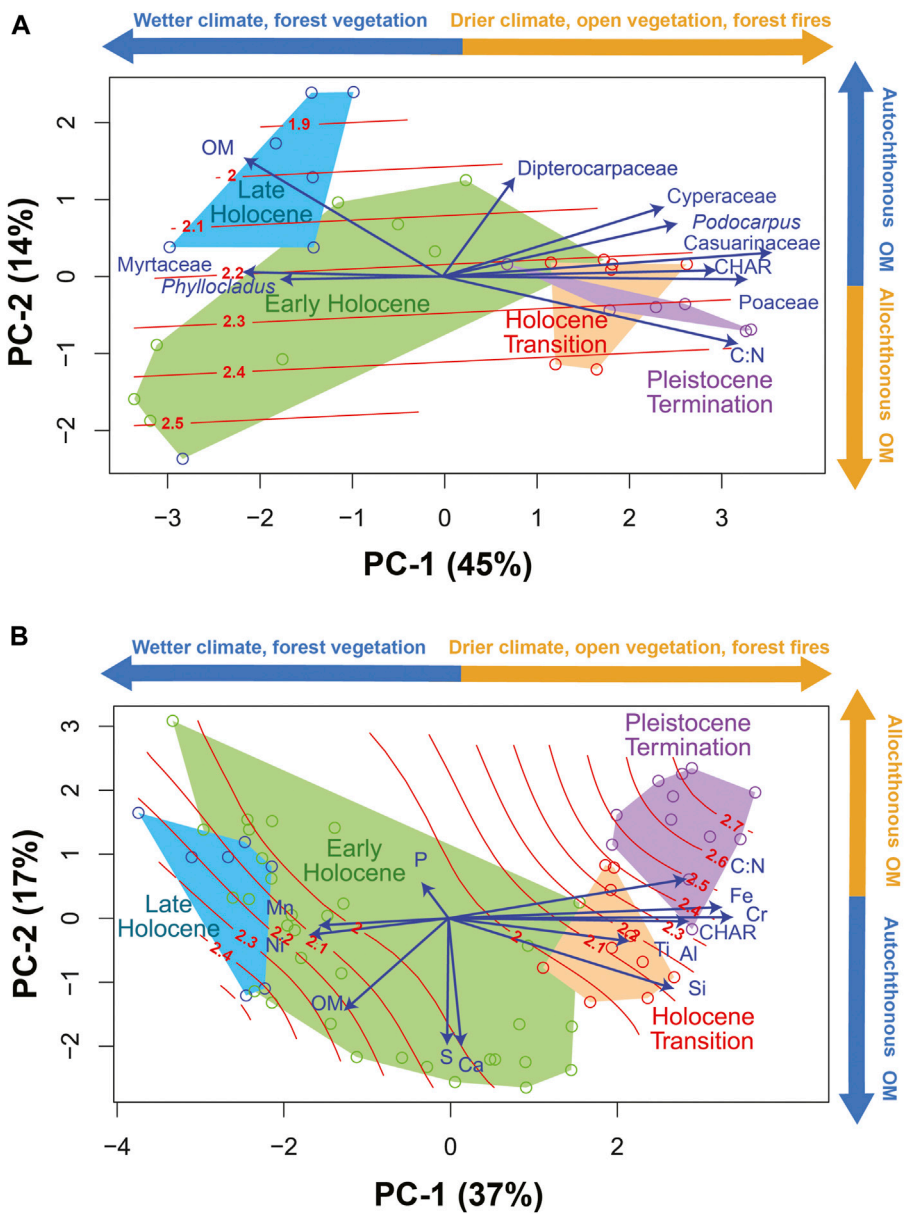

FIGURE 5
Principal Components Analysis of **(A)** charcoal flux, organic matter, C:N ratios and pollen and **(B)** charcoal flux, organic matter, C:N ratios and geochemistry from sediment samples of Lake Lantoa. A fitted surface (red) of mercury flux (μg m^{-2} yr^{-1}) is plotted passively within the ordination space using a thin-plate spline, indicating mercury's relationship to ordination scores.

The relatively high C:N ratios (μ = 23, 1σ = 2.28) indicate that there was still a significant amount of catchment-derived OM in the sediments. There is an increase in sulphur (S) counts from the Pleistocene Termination to the Holocene Transition, however manganese (Mn) and nickel (Ni) counts appear to remain similar between these two periods, suggesting that catchment input to the lake sediments was also similar (Hamilton et al., 2019b) (Figure 4). Therefore, the XRF counts indicate that the slight decrease in C:N ratios in the Holocene Transition was driven by an increase in primary productivity within the lake, rather than an increase in catchment input (Hamilton et al., 2019b).

The range in Hg concentrations and HgAR for the Holocene Transition decreased compared to the Pleistocene Termination (7.54 μg m^{-2} yr^{-1}, 1σ = 6.02 vs. 11.32 μg m^{-2} yr^{-1}, 1σ = 2.53, respectively, Table 2), a trend coeval with a decrease in CHAR compared to the Pleistocene Termination (0.34 m^{-2} yr^{-1}, 1σ = 0.25 vs. 0.59 m^{-2} yr^{-1}, 1σ = 0.21, respectively, Table 2). This trend in the Hg and CHAR records was likely driven by the progressive onset of increasingly humid conditions around the site during this period (Figure 4), reinforcing interpretations made from the pollen record (Hamilton et al., 2019b).

3.3.3 The Early Holocene (~11,700 to 5,000 cal BP; 321–110 cm)

The average HgAR in Lake Lantoa in the Early Holocene increased compared to the Holocene Transition (11.35 μg m^{-2} yr^{-1} vs. 7.54 μg m^{-2} yr^{-1}, respectively) and is marked by greater variability. The Early

Holocene has the highest average HgAR for the whole core, however this average is largely driven by isolated HgAR peaks within this period, with the highest peaks occurring at 8,015 cal BP (2,558 μg m^{-2} yr^{-1}) and 8,722 cal BP (1,029 μg m^{-2} yr^{-1}). When outliers are removed, the average HgAR is 6.30 μg m^{-2} yr^{-1}, similar to the Holocene Transition (7.54 μg m^{-2} yr^{-1}).

Our multiproxy data suggest two probable explanations for this increase in HgAR: 1) as this period is characterised by increasingly humid conditions in the Lake Lantoa catchment, flood pulses could have contributed to increasing Hg through in-wash of organic material from the catchment into the lake, including litterfall; and 2) as the Early Holocene is a period of intense volcanic activity in Southeast Asia (Ninkovich, 1979; Ku et al., 2009), volcanic emissions could also be a major contributor of Hg into the lake (either directly or via litterfall uptake and in-wash to the lake) (Figure 4).

The increases in S, Mn and Ni counts (Figure 4) are interpreted as an increase in catchment input to the sediments (Hamilton et al., 2019b). The decrease in C:N ratios (μ = 18, 1σ = 2.71) indicates that there was relatively more autochthonous OM in the sediments than in the Holocene Transition (μ = 23, 1σ = 2.58) or Pleistocene Termination (μ = 27, 1σ = 2.46 Table 2). These proxies (XRF counts, OM% and C:N ratio) demonstrate that there was an increase in catchment input to the lake sediments and lake primary productivity (Figure 4). This is reinforced by the pollen record, which illustrates that montane forest was expanding at this time (Figure 3) and represents the continuation of increasing humidity around the site (Hamilton et al., 2019b). We propose that the trends in the XRF counts and C:N ratios were driven by an increase in primary productivity within the lake, itself driven by increasing temperatures.

The environmental reconstruction for the Lake Lantoa catchment during the Early Holocene demonstrates a nuanced relationship between the proxies used in this study (Figure 5). The PCA results (Figure 5B) indicate that the catchment was less stable during the Early Holocene compared to the Holocene Transition. Indicators of catchment runoff and erosion in the Lake Lantoa sediments (S, Mn and Ni) are positively correlated with warmer and wetter conditions (Figure 5B), demonstrating that these conditions facilitate catchment input to the lake (Hamilton et al., 2019b). This relationship appears to be mediated by montane forest cover (Figure 3, Figure 5A).

3.3.4 The Late Holocene (~5,000–538 cal BP; 110–0 cm)

A marked difference in Hg concentrations and accumulation rates between the Early and Late Holocene can be seen in Lake Lantoa (Table 2, Figure 4). Average HgAR decreased during the Late Holocene compared to the Early Holocene (4 μg m^{-2} yr^{-1}, 1σ = 6.63 vs. 11 μg m^{-2} yr^{-1}, 1σ = 23.01, respectively), demonstrating the lowest average HgAR recorded in the entire core. This decrease is likely linked to an environmental shift at Lake Lantoa from wet climate conditions with an unstable catchment in the Early Holocene to wet conditions with a more stable catchment in the Late Holocene (Figure 3). This marked climate shift, dated at around 5,000 cal BP in Lake Lantoa, has been recorded globally in paleoclimate records from other parts of the world (Hermanns and Biester, 2013).

Organic matter (OM) increases distinctly in this period from the Early Holocene (μ = 23, 1σ = 2.32 vs. μ = 18, 1σ = 1.36, respectively), accompanied by a significant decrease in C:N ratios (μ = 14, 1σ = 2.17 vs. μ = 18, 1σ = 2.71, respectively), suggesting that the increase in OM during the Late Holocene was driven by a significant increase in primary productivity within the lake, rather than an increase in catchment input (Figure 4 and Table 2). The pollen record demonstrates a simultaneous increase in tropical forest cover during the Late Holocene (Figure 3), which appears to have promoted a more stable catchment (Hamilton et al., 2019b)).

The Late Holocene is characterised by established montane and lowland forests, suggesting that this period had the warmest and most humid conditions in the past 16,488 years. The significantly low C:N ratios for this period (Table 2), however, demonstrate that this period also received the lowest contribution of catchment input for the core. Therefore, while warmer and wetter conditions promote catchment runoff and erosion, vegetation establishment appears to mediate this relationship.

The significant increase in OM is concomitant with decreases in C:N ratios and HgAR during the Late Holocene. This decrease in HgAR and C:N (meaning more OM of autochthonous origin) suggest that the lake received less Hg input from the catchment, likely a result of a more established lowland forest. A decrease in HgAR means that the amount of Hg in the lake decreased (e.g., smaller Hg flux from the catchment), independent of Hg concentrations in the sediment. A more established forest (demonstrated by pollen data, Figure 5) means more stable soil, hindering Hg transfer from soil to the water phase. Alternatively, this decrease in HgAR could be a result of in-lake processes promoting Hg^{2+} reduction to Hg^0 and consequent Hg evasion, resulting in a decrease in the net Hg load to the lake. The link between primary productivity and HgAR in tropical lake sediments is poorly studied. More studies are needed to better understand the important relationship between lake-catchment dynamics, lake primary productivity and Hg deposition in freshwater lakes.

3.4 Main drivers of HgAR in Lake Lantoa sediments

The variability of HgAR in Lake Lantoa sediments appears to be heavily mediated by catchment dynamics such as vegetation cover and type, fire activities, and changes in precipitation. Previous studies have demonstrated the important role of vegetation and litterfall contributing to Hg concentrations in soils, a relationship mediated by vegetation type (Fostier et al., 2015; Zhang et al., 2016; Zheng et al., 2016; Zhang et al., 2019). Plant species, leaf age and leaf placement are biological factors that significantly influence Hg uptake by foliage (Laacouri et al., 2013; Zhu et al., 2016) and can be reflected in HgAR in lake sediments with densely vegetated catchments. While we recognise that changes in vegetation can influence HgAR in the lake, a this signal is indistinguishable from other signals and will not be discussed in this manuscript.

For a better spatial and temporal assessment of Hg patterns in our multi-proxy dataset, we plotted two principal component analyses (Figures 5A,B): the first is based on pollen data, and the second on geochemical data. Both graphs show the relationship between the ordination result and HgAR as an environmental variable. For the pollen PCA (Figure 5A), the samples from the Pleistocene Termination are positively loaded on axis 1 with open vegetation pollen taxa and charcoal, reinforcing that the dry climate and fire activity of the Pleistocene Termination were key drivers of HgAR. Mercury

TABLE 3 Comparison of the timing of peaks in mercury accumulation in Lake Lantoa sediments with the timing of volcanic eruptions reported for Southeast Asia (as reported in De Maisonneuve and Bergal-Kuvikas, 2020).

Mercury peak date (cal BP)	Potential source eruption (cal BP)	Volcano of origin	Reference
9,450 (10,056–9,434)	9,410 ± 150	Mount Pinatubo	Newhall et al. (1996)
8,722 (8,453–9,143)	Unknown	Banda Api and Banda Awu?	Global volcanism program, Smitsonian Institution, 2022
8,015 (7,611–8,304)	Unknown	Banda Api or Banda Awu?	Global volcanism program, Smitsonian Institution, 2022
6,254 (5,830–6,712)	6,875 ± 859	Taal Caldera	Martinez and Williams (1999)
5,708 (5,457–6,024)	5,500 ± 500	Mount Pinatubo	Newhall et al. (1996)
5,203 (4,887–5,453)	5,260 ± 780	Tengger caldera	Global volcanism program, Smitsonian Institution, 2022
5,107 (4,785–5,384)	5,479 ± 140	V5d eruption from unknown volcano	Salisbery et al. (2012)
4,769 (4,441–5,096)	4,860 ± 60	V5 eruption from unknown volcano	Salisbery et al. (2012)

sediment accumulation rates, passively plotted, have high concentrations during the Pleistocene Termination and Late Holocene, indicating the importance of fire and catchment runoff as drivers of HgAR in Lake Lantoa.

For the geochemistry PCA, Mn, Ni, S are negatively loaded on axis 1 (Figure 5B). These loadings are positioned in the Early Holocene area, at the time of several isolated HgAR peaks (likely of volcanic origin) and catchment runoff. Charcoal accumulation rates are loaded positively on axis 1, indicating a disconnect between fires and HgAR for the entire Holocene. This reinforces the interpretation that fires were unlikely to be primary contributors to Holocene HgAR in Lake Lantoa.

3.5 Possible volcanic contributions to mercury deposition in Lake Lantoa

The isolated peaks in Hg concentrations and accumulation rates in Lake Lantoa during the Early Holocene do not appear to be driven by lake-catchment processes. These peaks are associated with low fire activities, indicating that forest fires were not a major contributor to these peaks (Figure 3). This is supported by the pollen record which demonstrates that the Lake Lantoa catchment experienced warm and wet climate conditions during the Early Holocene (Figure 3) (Hamilton et al., 2019b). Furthermore, there are no significant abrupt perturbations in any of the other proxy records for Lake Lantoa (Figure 3; Figure 4) which suggest that these peaks in the Hg record are being driven by external catchment processes. We propose that a process that would result in an unsustained drastic increase in Hg deposition in the Lake Lantoa sediments, with minor impact on proxies of lake-catchment dynamics, is volcanism. That is not to say that is the only possible external process that could result in a significant abrupt increase in HgAR, however, given the high volcanic activity of the SEA region it appears to be the most reasonable explanation. Further exploration of this theory is outside the scope of this paper, however we do present a series of hypotheses that can be used to assess the validity of this theory.

A valid explanation for four statistically significant peaks in the Hg record (43 μg m^{-2} yr^{-1} at 5,203 cal BP, 37 μg m^{-2} yr^{-1} at 5,708 cal BP, 158 μg m^{-2} yr^{-1} at 8,015 cal BP, and 68 μg m^{-2} yr^{-1} at 1,029 cal BP) should be able to address why these peaks are two standard deviations above the average HgAR for the entire core (μ = 9, 1σ = 13.30). Figures 3 and 4 demonstrate that there are no perturbations in the multiproxy record proportional to the Hg peaks, further supporting the theory that these peaks are driven by processes that other proxies are not sensitive enough to capture.

Volcanic degassing and eruptions primarily emit mercury in its elemental form, Hg(0) (Ansmann et al., 1997; Slemr and Scheel, 1998; Polvani et al., 2019). In this form, Hg can be transported long distances from the original emission source (Ci et al., 2011). The following discussion explores the feasibility of regional volcanism contributing to the Lake Lantoa Hg record.

To facilitate future investigations aimed at identifying sources of volcanic Hg in the region, Table 3 presents known volcanic eruptions in SEA (as reported by De Maisonneuve and Bergal Kuvikas, 2020) coincident with eight distinct peaks in the Hg record. More data is needed to confirm the drivers of these isolated extrusions in the Hg record (Table 3), which may be outside of the SEA region.

Several volcanoes in Southeast Asia could have contributed to higher HgAR in Lake Lantoa sediments during the Early Holocene (Figure 6). As atmospheric pressure gradients are weak in the tropics (Phadke et al., 2003), the wind is variable and can transport Hg emitted by volcanoes in several directions (Figure 6). Known eruptions for the early Holocene period for Southeast Asia are presented in Figure 7 together with geochemical proxies for the LL2 core. The trend in elements seen from the XRF counts indicate strong variability during the Early Holocene, supported by high S counts. The above hypothesis could be supplemented by a secondary study investigating instrumental differences in tracking volcanic emissions, and focusing on elements of volcanic origin such as sulphur.

The validity of our hypothesis that isolated peaks in the Lake Lantoa Hg record during the Early Holocene were driven by volcanism could be investigated by comparing the geochemical fingerprint of the eruption and the geochemical fingerprint of the sediments associated with the Hg peaks in question. Studies could

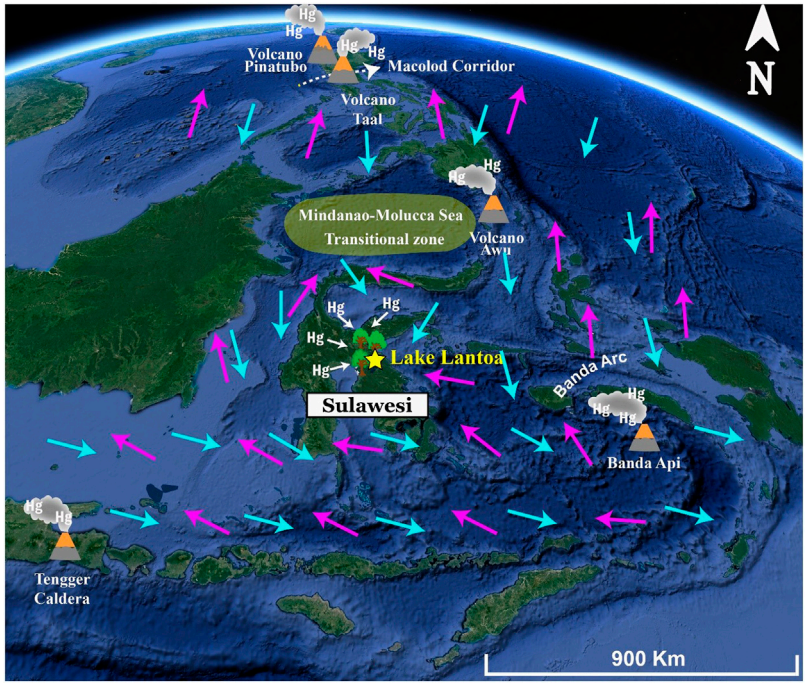

FIGURE 6
Location of Southeast Asia volcanoes with potential mercury (Hg) emission and transport to Lake Lantoa (yellow star) in the early Holocene. Trees represent dry Hg deposition throught litterfall. Cyan arrows indicate the direction of monsoon winds toward east-southeast during wet season (mean wind direction January 1946–1989). Pink arrows indicate the direction of monsoon winds toward north-northwest during dry season (mean wind direction August 1946–1989). Wind data adapted from Klicpera and Westphal. (2017) and originally derived from COADS Monthly Climatology dataset (Woodruff et al., 1998).

also use different methods of characterising soil geochemistry (e.g., Inductively Coupled Plasma Mass Spectrometry vs. Laser Ablation Inductively Coupled Plasma Mass Spectrometry vs. XRF) to assess if one method is more sensitive to regional (vs. local) events.

Such studies would benefit from a modelling study to demonstrate the transportation and subsequent fallout and deposition of volcanic emissions, mediated by changes in trade winds. They would also clarify the plausibility of regional volcanism impacting the Hg record in Lake Lantoa without affecting the XRF or pollen records. These studies might also indicate which elements/molecules/compounds are best suited to tracking the range of volcanic emissions from a given eruption.

It is important to note that no reported eruptions in SEA for this period were found in the literature for the two highest peaks in HgAR for the entire LL2 core (at ~ 8,015 cal BP and ~8,722 cal BP). These peaks in HgAR (158 μg m^{-2} yr^{-1} and 68 μg m^{-2} yr^{-1} respectively) are ~13 and 6 times higher than the average HgAR (11.35 μg m^{-2} yr^{-1}) for the Early Holocene (Table 2). The suggestions mentioned above may be able to clarify which, if any, volcanoes could have contributed to these Hg peaks. Two Hg peaks are coeval with eruptions of Mount Pinatubo in the Philippines (Table 3, Figure 7): the eruptions of 9,410 ± 150 and 5,500 ± 500 cal BP (Newhall et al., 1996). We use the dominant direction of ash cloud distribution to infer the direction of volcanic gas transportation, including Hg(0), for the 9,410 ± 150 cal BP eruption. The ash cloud associated with this eruption is distributed southwest of the Philippines (De Maisonneuve and Bergal-Kuvikas, 2020), implying that Hg emissions from volcanoes in the Philippines could have been transported to Indonesia.

The Hg peak at ~ 4,769 cal BP potentially corresponds to the 4,860 ± 60 cal BP V5 eruption, which is recorded in a marine core close to Sumatra (Salisbury et al., 2012). The authors report one significant ash layer (V5) dating to 4,860 ± 60 BP and another ash layer (V5d) dating to 5,479 ± 140 BP was identified in another core (Salisbery et al., 2012).

The potential contribution of volcanic events listed in Figure 7 to the Lake Lantoa Hg record could be investigated via fingerprinting the chemical signature of these eruptions. Modelling studies examining the transportation and subsequent fallout and deposition of volcanic emissions, mediated by changes in trade winds, would also clarify the plausibility of regional volcanism impacting the Hg record in Lake Lantoa without affecting the XRF or pollen records.

Fingerprinting a potential eruption for these Hg peaks is difficult considering the limited number of studies on pre-historic eruptions or tephra layers documented in Indonesia (De Maisonneuve and Bergal-Kuvikas, 2020). The Hg peaks could be either a result of secondary catchment processes and reworked material being transported to the lake, or a case of unknown volcanic sources. The Banda Api and Banda Awu calderas, both in the Sunda-Banda arc, are believed to have erupted during this period. These two calderas are near Lake Lantoa (Figure 6) and of a significant size: Banda Api caldera is 7 km wide and Banda Awu 4.5 km wide (Smithsonian Institution, 2020). Unfortunately, there is no information on the dates of their caldera-forming eruptions or spatial distributions of pyroclastic deposits. Despite the abundance of

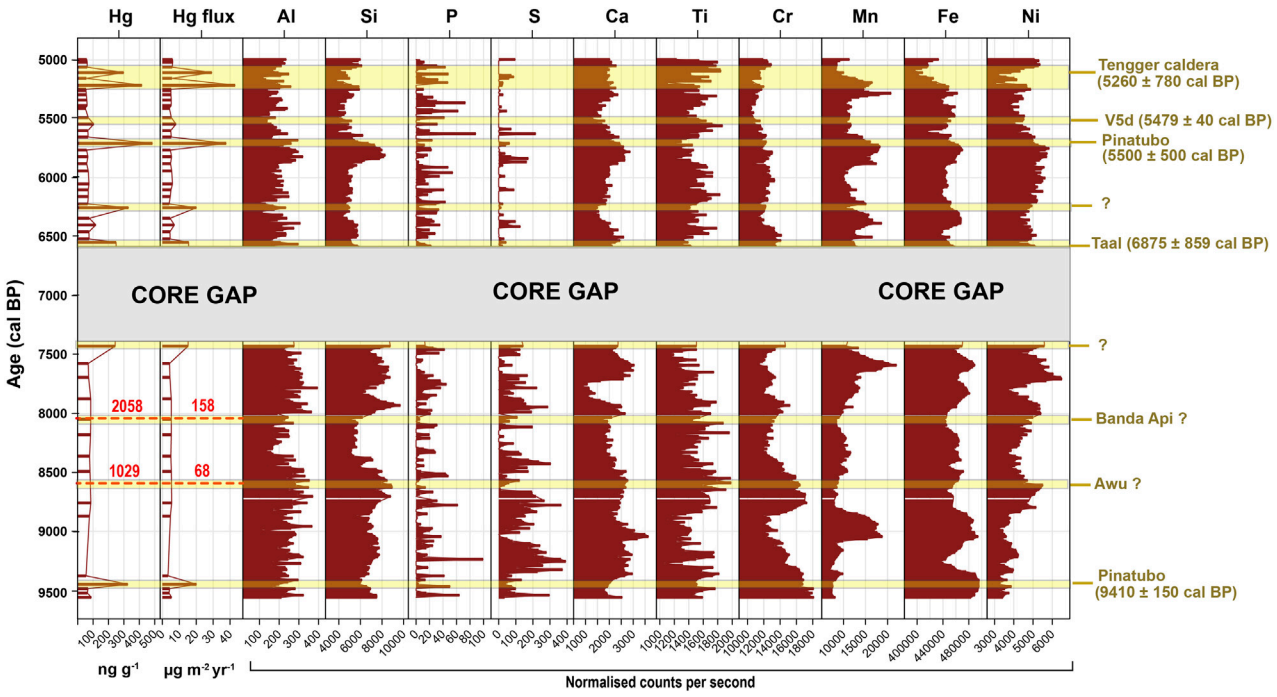

FIGURE 7
Geochemical profile for the early-mid Holocene at Lake Lantoa, showing mercury profile and known volcanic eruptions that could potentially have contributed to mercury inputs. Mercury peaks are highlighted in yellow, and known volcanic eruptions are indicated on the right of the figure. The two highest peaks in Hg and HgAR (at 8,015 and 8,722 cal BP) were removed for clearer plotting of these proxies. They are represented as red dashed lines with their values and are plotted off scale.

volcanoes recorded Southeast Asia (147 alone in Indonesia, according to Hariyono and Liliasari, 2018), Banda Api and Banda Awu are the most promising candidates due to their location and wind direction, and further studies should investigate these two volcanoes as significant potential Hg sources for Sulawesi.

Two other Hg peaks (at ~7,429 and 6,254 cal BP) also do not correspond to any known volcanic eruptions. This highlights the gap in our understanding of the role secondary catchment processes have on HgAR in tropical lakes. For instance, soil acidification from volcanic aerosols can cause significant leaching of nutrients after volcanic eruptions (Yagasaki et al., 2006; Guédron et al., 2019). This is particularly a problem in the Lake Lantoa catchment, where ultramafic soils are reported to be already nutrient poor (Van der Ent et al., 2013). Extreme nutrient limitation and increase in sulphur input can trigger a breakdown in forest vegetation, with trees losing foliage and widespread soil erosion (Guédron et al., 2019). This may have been the case in Lake Lantoa at the time of major Hg input pulses to the lake. The sulphur counts for LL2 appear to support this hypothesis, with the highest counts at recorded during the Early Holocene relative to the rest of the core (Figure 4).

The acidification of Indonesian soils as a result of volcanic activities has been reported for the island of Sumatra (Setyaningsih et al., 2018). In this case, volcanic activities reduced vegetation diversity with volcanophile taxa (e.g., Casuarinaceae and Myrtaceae) thriving and other rainforest taxa only outcompeting the volcanophile taxa several centuries after volcanic deposition ceased (Setyaningsih et al., 2018). This pattern results from the volcanic aerosols depleting the soils of nitrogen, with Casuarinaceae and Myrtaceae better adapted to these soils than rainforest taxa (Setyaningsih et al., 2018). It should also be noted that rainforest taxa may take longer to recover after volcanic deposition and deforestation, relative to volcanophile taxa, due to the change in the amount of sunlight reaching the ground, as many require semi-shaded areas to germinate or establish.

The impact of soil acidification from volcanic activities may be compounded if the area is dominated by taxa that do not thrive in nitrogen-depleted soils, like *Podocarpus* (Li et al., 2021). These conditions promote litterfall and organic decomposition of these taxa, facilitated by the warm temperatures and humid climate of the tropics, which has direct implications for Hg sequestered in catchment soils that can be transported into the lake through catchment runoff (Guédron et al., 2019). The effects of ash cover on vegetation, germination and establishment must also be considered, however, a comprehensive analysis of the relationship between volcanic activity and lake-catchment dynamics is outside the scope of this paper.

4 Conclusions and future directions

This study presents the first long-term record of HgAR in a tropical lake in Southeast Asia (SEA). It is also one of the few studies globally to combine Hg records with a comprehensive set of ecological and geochemical data (i.e., pollen, charcoal, multi-element geochemistry, and C:N ratio). The results describe a dynamic relationship between HgAR, lake-catchment conditions,

forest fires and regional volcanism. These relationships are mediated by climate conditions which can promote or inhibit the accumulation of Hg in lake sediments.

Our results indicate that the highest HgAR in Lake Lantoa are associated with high seasonality (i.e., the catchment experiences both fire and high precipitation events annually), wet climates (i.e., flood pulse events) and an unstable catchment area. Established forest taxa have the greatest capacity to uptake and sequester atmospheric Hg, reducing the amount of Hg deposited on surface soils that can be re-deposited into the lake via precipitation or flood events. Therefore, non-seasonal climates with established forests are likely to act as long-term Hg sinks, reducing Hg accumulation in lake sediments. These results suggest that areas with non-seasonal wet climates in established forests serve as long-term Hg sinks. Therefore, shifts in climate to drier and more variable conditions in these areas have the potential to trigger a dramatic increase in Hg accumulation into aquatic systems and the atmosphere.

Additionally, the Lake Lantoa record reinforces studies demonstrating that algae production can bio-dilute Hg accumulation in lake sediments (e.g., Outridge et al., 2019). The C:N ratios dramatically decrease while OM% dramatically increases during the Late Holocene, indicating a significant rise in autochthonous OM in lake sediments, which is attributed to an increase in primary productivity (Figure 3). This shift in primary productivity proxies is associated with the lowest HgAR for the entire core (Table 2). This suggests that a more stable catchment hindering Hg inputs to the lake, or inlake processes resulting in Hg evasion.

Volcanism appears to be an important source of Hg to Lake Lantoa, via both direct (atmospheric) and secondary (terrestrial) HgAR. More datasets from the SEA region would elucidate the response of HgAR to the interplay between volcanism and ecological processes. More studies fingerprinting eruption signals in SEA sediments are needed to further examine this relationship.

Data availability statement

The original contributions presented in the study are included in the article/Supplementary Material, further inquiries can be directed to the corresponding author.

Author contributions

JN–analysis, acquisition and interpretation of the mercury record and comparison with new and published geochemical and palynological records. LS–drafting and critical revision of the manuscript and interpretation of the mercury record, and comparison of southern hemisphere mercury records. RH–acquisition, analysis and interpretation of the palynological (pollen and charcoal) and XRF-scanning records, approval for publication of the content. SC–drafting and critical revision of the manuscript, assisted with selection of pollen data relevant to understanding the mercury record. HB - drafting and critical revision of the manuscript and interpretation of the mercury record. HS-W–acquisition, analysis and interpretation of the Carbon:Nitrogen ratio data. OB-K–interpretation of the mercury and XRF record, particularly with reference to possible volcanic sources of mercury peaks in the Holocene. GJ–acquisition, analysis and interpretation of the age-depth model. JS–acquisition of the LL2 sediment core, analysis and interpretation of the palynological record, approval for publication of the content. All authors contributed to the article and approved the submitted version.

Funding

This project has been funded by the Australian Research Council Discovery Early Career Researcher Award (DE180100573) granted to LS. The original recovery of the Lake Lantoa material was carried out under RISTEK permit number 267 and Australian Research Council Funding (DP110101357) to JS. AMS radiocarbon dates at ANSTO were funded by ANSTO Research grant AP12188 to RH.

Acknowledgments

We acknowledge the financial support from the Australian Government for the Centre for Accelerator Science at ANSTO through the National Collaborative Research Infrastructure Strategy (NCRIS). Thanks are given to the office of Bupati Luwu Timur as well as Camat Nuha and Camat Towuti and to the Mahalona community for their consent, hospitality and logistical support.

Conflict of interest

Author HB was employed by AG Umweltgeochemie.

The remaining authors declare that the research was conducted in the absence of any commercial or financial relationships that could be construed as a potential conflict of interest.

Publisher's note

Supplementary material

The Supplementary Material for this article can be found online at: https://www.frontiersin.org/articles/10.3389/fenvc.2023.1241176/full#supplementary-material

References

Amirbahman, A., Ruck, P. L., Fernandez, I. J., Haines, T. A., and Kahl, J. S. (2004). The effect of fire on mercury cycling in the soils of forested watersheds: acadia National Park, Maine, U.S.A. *Water, Air, Soil Pollut.* 152 (1-4), 315–331. doi:10.1023/b:wate.0000015369.02804.15

Anhuf, D., Ledru, M. P., Behling, H., Da Cruz, F., Cordeiro, R., Van der Hammen, T., et al. (2006). Paleo-environmental change in Amazonian and African rainforest during the LGM. *Palaeogeogr. Palaeoclimatol. Palaeoecol.* 239, 510–527. doi:10.1016/j.palaeo.2006.01.017

Ansmann, A., Mattis, I., Wandinger, U., Wagner, F., Reichardt, J., and Deshler, T. (1997). Evolution of the Pinatubo aerosol: raman lidar observations of particle optical depth, effective radius, mass, and surface area over central Europe at 53.4°N. *J. Atmos. Sci.* 54 (22), 2630–2641. doi:10.1175/1520-0469(1997)054<2630:EOTPAR>2.0.CO;2

Benson, L., Burdett, J., Lund, S., Kashgarian, M., and Mensing, S. (1997). Nearly synchronous climate change in the Northern Hemisphere during the last glacial termination. *Nature* 388, 263–265. doi:10.1038/40838

Blaauw, M., and Christen, J. A. (2011). Flexible paleoclimate age-depth models using an autoregressive gamma process. *Bayesian Anal.* 6, 457–474. doi:10.1214/11-ba618

Caffrey, M. A., and Horn, S. P. (2013). The use of lithium heteropolytungstate in the heavy liquid separation of samples which are sparse in pollen. *Palynology* 37 (1), 143–150. doi:10.1080/01916122.2012.736417

Chabangborn, A., Brandefelt, J., and Wohlfarth, B. (2014). Asian monsoon climate during the Last Glacial Maximum: palaeo-data-model comparisons. *Boreas* 43 (1), 220–242. doi:10.1111/bor.12032

Ci, Z., Zhang, X., Wang, Z., and Niu, Z. (2011). Atmospheric gaseous elemental mercury (GEM) over a coastal/rural site downwind of East China: temporal variation and long-range transport. *Atmos. Environ.* 45 (15), 2480–2487. doi:10.1016/j.atmosenv.2011.02.043

Colinvaux, P. A., De Oliveira, P. E., Moreno, J. E., Miller, M. C., and Bush, M. B. (1996). A long pollen record from lowland Amazonia: forest and cooling in glacial times. *Science* 274 (5284), 85–88. doi:10.1126/science.274.5284.85

Core Team (2013). *R: a language and environment for statistical computing*. Vienna: R: A language and environment for statistical computing.

Costa, K. M., Russell, J., Vogel, H., and Bijaksana, S. (2015). Hydrological connectivity and mixing of Lake Towuti, Indonesia in response to paleoclimatic changes over the last 60,000 years. *Palaeogeogr. Palaeoclimatol. Palaeoecol.* 417, 467–475. doi:10.1016/j.palaeo.2014.10.009

Daga, R., Ribeiro Guevara, S., Pavlin, M., Rizzo, A., Lojen, S., Vreča, P., et al. (2016). Historical records of mercury in southern latitudes over 1600 years: lake Futalaufquen, Northern Patagonia. *Sci. Total Environ.* 553, 541–550. doi:10.1016/j.scitotenv.2016.02.114

Davies, S. J., Lamb, H. F., and Roberts, S. J. (2015). "Micro-XRF Core Scanning in Palaeolimnology: recent Developments," in *Micro-XRF studies of sediment cores: applications of a non-destructive tool for the environmntal sciences* (Netherlands: Springer), 189–226. doi:10.1007/978-94-017-9849-5_7

De Deckker, P. (2016). The Indo-Pacific Warm Pool: critical to world oceanography and world climate. *Geosci. Lett.* 3, 20. doi:10.1186/s40562-016-0054-3

De Maisonneuve, C. B., and Bergal-Kuvikas, O. (2020). Timing, magnitude and geochemistry of major Southeast Asian volcanic eruptions: identifying tephrochronologic markers. *J. Quat. Sci.* 35 (1–2), 272–287. doi:10.1002/jqs.3181

Demers, J. D., Blum, J. D., and Zak, D. R. (2013). Mercury isotopes in a forested ecosystem: implications for air-surface exchange dynamics and the global mercury cycle. *Glob. Biogeochem. Cycles* 27 (1), 222–238. doi:10.1002/gbc.20021

Devesa-Rey, R., and Barral, M. T. (2012). Allochthonous versus autochthonous naturally occurring organic matter in the Anllóns river bed sediments (Spain). *Environ. Earth Sci.* 66 (3), 773–782. doi:10.1007/s12665-011-1286-3

Engstrom, D. R., Balogh, S. J., and Swain, E. B. (2007). History of mercury inputs to Minnesota lakes: influences of watershed disturbance and localized atmospheric deposition. *Limnol. Oceanogr.* 52 (6), 2467–2483. doi:10.4319/lo.2007.52.6.2467

Enrico, M., Roux, G. L., Marusczak, N., Heimbürger, L. E., Claustres, A., Fu, X., et al. (2016). Atmospheric Mercury Transfer to Peat Bogs Dominated by Gaseous Elemental Mercury Dry Deposition. *Environ. Sci. Technol.* 50 (5), 2405–2412. doi:10.1021/acs.est.5b06058

Fadina, O. A., Venancio, I. M., Belem, A., Silveira, C. S., Bertagnolli, D. d. C., Silva-Filho, E. V., et al. (2019). Paleoclimatic controls on mercury deposition in northeast Brazil since the Last Interglacial. *Quat. Sci. Rev.* 221, 105869. doi:10.1016/j.quascirev.2019.105869

Fægri, K., and Iverson, J. (1989). *Textbook of pollen analysis*. 4th edn. Chester, UK: John Wiley & Sons, Ltd.

Fisher, J. A., and Nelson, P. F. (2020). Atmospheric mercury in Australia: recent findings and future research needs. *Elementa* 8, 1–20. doi:10.1525/elementa.2020.070

Fostier, A. H., Melendez-Perez, J. J., and Richter, L. (2015). Litter mercury deposition in the Amazonian rainforest. *Environ. Pollut.* 206, 605–610. doi:10.1016/j.envpol.2015.08.010

Guédron, S., Tolu, J., Brisset, E., Sabatier, P., Perrot, V., Bouchet, S., et al. (2019). Late Holocene volcanic and anthropogenic mercury deposition in the western Central Andes (Lake Chungará, Chile). *Sci. Total Environ.* 662, 903–914. doi:10.1016/j.scitotenv.2019.01.294

Hamilton, R., Hall, T., Stevenson, J., and Penny, D. (2019a). Distinguishing the pollen of Dipterocarpaceae from the seasonally dry and moist tropics of south-east Asia using light microscopy. *Rev. Palaeobot. Palynology* 263, 117–133. doi:10.1016/j.revpalbo.2019.01.012

Hamilton, R., Stevenson, J., Stevenson, J., and Bijaksana, S. (2019b). A 16,000-year record of climate, vegetation and fire from Wallacean lowland tropical forests. *Quat. Sci. Rev.* 224, 105929. doi:10.1016/j.quascirev.2019.105929

Hamilton, R., and Stevenson, J. (2020). The challenge of the enigmatic tricolporate tropical pollen type: A case study from Sulawesi, Indonesia. *Rev. Palaeobot. Palynology* 273, 104146–104221. doi:10.1016/j.revpalbo.2019.104146

Hariyono, E., and Liliasari, S. (2018). "The Characteristics of Volcanic Eruption in Indonesia," in *Volcanoes - geological and geophysical setting, theoretical aspects and numerical modeling, applications to industry and their impact on the human health* (London: IntechOpen). doi:10.5772/intechopen.71449

Hermanns, Y. M., and Biester, H. (2013). A 17,300-year record of mercury accumulation in a pristine lake in southern Chile. *J. Paleolimnol.* 49 (4), 547–561. doi:10.1007/s10933-012-9668-4

Hogg, A., Heaton, T. J., Hua, Q., Palmer, J. G., Turney, C. S., Southon, J., et al. (2020). SHCal20 Southern Hemisphere Calibration, 0–55,000 Years cal BP. *Radiocarbon* 62 (4), 759–778. doi:10.1017/RDC.2020.59

Hope, G. (2001). Environmental change in the late Pleistocene and later Holocene at wanda site, soroako, South Sulawesi, Indonesia. *Palaeogeogr. Palaeoclimatol. Palaeoecol.* 171 (3–4), 129–145. doi:10.1016/S0031-0182(01)00243-7

Huang, T.-C. (1972). *Pollen flora of taiwan*. Taiwan: National Taiwan University Botany Department Press.

Jiskra, M., Wiederhold, J. G., Skyllberg, U., Kronberg, R. M., Hajdas, I., and Kretzschmar, R. (2015). Mercury Deposition and Re-emission Pathways in Boreal Forest Soils Investigated with Hg Isotope Signatures. *Environ. Sci. Technol.* 49 (12), 7188–7196. doi:10.1021/acs.est.5b00742

Ku, Y. P., Chen, C. H., Song, S. R., Iizuka, Y., and Shen, J. J. S. (2009). A 2 Ma record of explosive volcanism in southwestern Luzon: implications for the timing of subducted slab steepening. *Geochem. Geophys. Geosystems* 10 (6), 2486. doi:10.1029/2009GC002486

Laacouri, A., Nater, E. A., and Kolka, R. K. (2013). Distribution and Uptake Dynamics of Mercury in Leaves of Common Deciduous Tree Species in Minnesota, U.S.A. *Environ. Sci. Technol.* 47 (18), 10462–10470. doi:10.1021/es401357z

Labrière, N., Locatelli, B., Laumonier, Y., Freycon, V., and Bernoux, M. (2015). Soil erosion in the humid tropics: A systematic quantitative review. *Agric. Ecosyst. Environ.* 203, 127–139. doi:10.1016/j.agee.2015.01.027

Lacerda, L. D., Ribeiro, M. G., and Sifeddine, A. (1999). Atmospheric mercury deposition over Brazil during the past 30,000 years. *Cienc. Cult.* 30, 000.

Lacerda, L. D., Turcq, B., Sifeddine, A., and Cordeiro, R. C. (2017). Mercury accumulation rates in Caço Lake, NE Brazil during the past 20.000 years. *J. S. Am. Earth Sci.* 77, 42–50. doi:10.1016/j.jsames.2017.04.008

Lal, R. (1990). *Soil erosion in the tropics: principles and management*. New York: McGraw-Hill.

Li, R., Han, J., Zhu, L., Zhao, L., Huang, X., Zhang, M., et al. (2021). Does nitrogen fertilization impact nonstructural carbohydrate storage in evergreen Podocarpus macrophyllus saplings? *J. For. Res.* 32 (4), 1653–1661. doi:10.1007/s11676-020-01181-z

Lindberg, S., Bullock, R., Ebinghaus, R., Engstrom, D., Feng, X., Fitzgerald, W., et al. (2007). A Synthesis of Progress and Uncertainties in Attributing the Sources of Mercury in Deposition. *Ambio* 36 (1), 19–33. doi:10.1579/0044-7447(2007)36[19:asopau]2.0.co;2

Lindberg, S. E., and Stratton, W. J. (1998). Atmospheric mercury speciation: concentrations and behavior of reactive gaseous mercury in ambient air. *Environ. Sci. Technol.* 32 (1), 49–57. doi:10.1021/es970546u

Lintern, A., Schneider, L., Beck, K., Mariani, M., Fletcher, M. S., Gell, P., et al. (2020). Background concentrations of mercury in Australian freshwater sediments: the effect of catchment characteristics on mercury deposition. *Elementa* 8 (1), 19. doi:10.1525/elementa.019

Martinez, M. M. L., and Williams, S. N. (1999). "Basaltic andesite to andesite scoria pyroclastic flow deposits from Taal caldera, Philippines." *Journal of Geological Society Philippines* 54 (1 & 2), 1–18.

Melack, J. M., and Forsberg, B. R. (2001). "Biogeochemistry of the Amazon Floodplain," in *The biogeochemistry of the amazon basin*. Editors M. E. McClain, R. Victoria, and J. E. Richey (New York: Oxford University Press), 235–274. doi:10.1093/oso/9780195114317.003.0017

Newhall, C., Dagg, A. S., and Delfin, F. G. (1996). "Eruptive History of Mount Pinatubo," in *Fire and mud. Eruptions and lahars of Mount Pinatubo, Philippines.*

Editor R. Punongbayan (Seattle: University of Washington Press and Philippine Institute of Volcanology and Seismology), 165–195.

Ninkovich, D. (1979). Distribution, age and chemical composition of tephra layers in deep-sea sediments off Western Indonesia. *J. Volcanol. Geotherm. Res.* 5, 67–86. doi:10.1016/0377-0273(79)90033-7

Obrist, D., Agnan, Y., Jiskra, M., Olson, C. L., Colegrove, D. P., Hueber, J., et al. (2017). Tundra uptake of atmospheric elemental mercury drives Arctic mercury pollution. *Nature* 547 (7662), 201–204. doi:10.1038/nature22997

Obrist, D., Kirk, J. L., Zhang, L., Sunderland, E. M., Jiskra, M., and Selin, N. E. (2018). A review of global environmental mercury processes in response to human and natural perturbations: changes of emissions, climate, and land use. *Ambio* 47 (2), 116–140. doi:10.1007/s13280-017-1004-9

Outridge, P. M., Sanei, H., Stern, H., and Goodarzi, F. (2007). Evidence for control of mercury accumulation rates in Canadian High Arctic lake sediments by variations of aquatic primary productivity. *Environ. Sci. Technol.* 41 (15), 5259–5265. doi:10.1021/es070408x

Outridge, P. M., Stern, G. A., Hamilton, P. B., and Sanei, H. (2019). Algal scavenging of mercury in preindustrial Arctic lakes. *Limnol. Oceanogr.* 64 (4), 1558–1571. doi:10.1002/lno.11135

Parkman, H., and Meili, M. (1992). Mercury in Macroinvertebrates from Swedish Forest Lakes: influence of Lake Type, Habitat, Life Cycle, and Food Quality. *Can. J. Fish. Aquat. Sci.* 50, 521–534. doi:10.1139/f93-061

Partin, J. W., Quinn, T., Shen, C. C., Okumura, Y., Cardenas, M., Siringan, F., et al. (2015). Gradual onset and recovery of the Younger Dryas abrupt climate event in the tropics. *Nat. Commun.* 6, 8061. doi:10.1038/ncomms9061

Pérez-Rodríguez, M., and Biester, H. (2022). Sensitivity of river catchments to discharge-controlled dissolved carbon export: a study of eight catchments in southern Patagonia. *Biogeochemistry* 160 (2), 177–197. doi:10.1007/s10533-022-00947-3

Pérez-Rodríguez, M., Horák-Terra, I., Rodríguez-Lado, L., Aboal, J. R., and Martínez Cortizas, A. (2015). Long-Term (~57 ka) controls on mercury accumulation in the souther hemisphere reconstructed using a peat record from pinheiro mire (minas gerais, Brazil). *Environ. Sci. Technol.* 49 (3), 1356–1364. doi:10.1021/es504826d

Phadke, A. C., Martino, C. D., Cheung, K. F., and Houston, S. H. (2003). Modeling of tropical cyclone winds and waves for emergency management. *Ocean. Eng.* 30, 553–578. doi:10.1016/s0029-8018(02)00033-1

Polvani, L. M., Banerjee, A., and Schmidt, A. (2019). Northern Hemisphere continental winter warming following the 1991 Mt. Pinatubo eruption: reconciling models and observations. *Atmos. Chem. Phys.* 19 (9), 6351–6366. doi:10.5194/acp-19-6351-2019

Power, M. J., Marlon, J., Ortiz, N., Bartlein, P. J., Harrison, S. P., Mayle, F. E., et al. (2008). Changes in fire regimes since the last glacial maximum: an assessment based on a global synthesis and analysis of charcoal data. *Clim. Dyn.* 30 (7–8), 887–907. doi:10.1007/s00382-007-0334-x

Renssen, H., Goosse, H., Roche, D. M., and Seppä, H. (2018). The global hydroclimate response during the Younger Dryas event. *Quat. Sci. Rev.* 193, 84–97. doi:10.1016/j.quascirev.2018.05.033

Ribeiro Guevara, S., Meili, M., Rizzo, A., Daga, R., and Arribére, M. (2010). Sediment records of highly variable mercury inputs to mountain lakes in Patagonia during the past millennium. *Atmos. Chem. Phys.* 10 (7), 3443–3453. doi:10.5194/acp-10-3443-2010

Riddle, B., Fox, J., Mahoney, D. T., Ford, W., Wang, Y. T., Pollock, E., et al. (2022). Considerations on the use of carbon and nitrogen isotopic ratios for sediment fingerprinting. *Sci. Total Environ.* 817 (152640), 152640–152719. doi:10.1016/j.scitotenv.2021.152640

Roulet, M., Lucotte, M., Saint-Aubin, A., Tran, S., Rhéault, I., Farella, N., et al. (1998). The geochemistry of mercury in central Amazonian soils developed on the Alter-do-Chão formation of the lower Tapajós River Valley, Pará state, Brazil. *Sci. Total Environ.* 223, 1–24. doi:10.1016/s0048-9697(98)00265-4

Russell, J. M., Bijaksana, S., Vogel, H., Melles, M., Kallmeyer, J., Ariztegui, D., et al. (2016). The Towuti Drilling Project: paleoenvironments, biological evolution, and geomicrobiology of a tropical Pacific lake. *Sci. Drill.* 21, 29–40. doi:10.5194/sd-21-29-2016

Russell, J. M., Vogel, H., Bijaksana, S., Melles, M., Deino, A., Hafidz, A., et al. (2020). The late quaternary tectonic, biogeochemical, and environmental evolution of ferruginous Lake Towuti, Indonesia. *Palaeogeogr. Palaeoclimatol. Palaeoecol.* 556, 109905. doi:10.1016/j.palaeo.2020.109905

Russell, J. M., Vogel, H., Konecky, B. L., King, J. W., Huang, Y., Melles, M., et al. (2014). Glacial forcing of central Indonesian hydroclimate since 60,000 y B.P. *PNAS* 111 (14), 5100–5105. doi:10.1073/pnas.1402373111

Salisbury, M. J., Patton, J. R., Kent, A. J., Goldfinger, C., Djadjadihardja, Y., and Hanifa, U. (2012). Deep-sea ash layers reveal evidence for large, late Pleistocene and Holocene explosive activity from Sumatra, Indonesia. *J. Volcanol. Geotherm. Res.* 231 (232), 61–71. doi:10.1016/j.jvolgeores.2012.03.007

Schneider, L., Cooke, C. A., Stansell, N. D., and Haberle, S. G. (2020). Effects of climate variability on mercury deposition during the Older Dryas and Younger Dryas in the Venezuelan Andes. *J. Paleolimnol.* 63 (3), 211–224. doi:10.1007/s10933-020-00111-7

Schneider, L., Fisher, J. A., Diéguez, M. C., Fostier, A. H., Guimaraes, J. R. D., Leaner, J. J., et al. (2023). A synthesis of mercury research in the Southern Hemisphere, part 1: natural processes. *Ambio* 52, 897–917. doi:10.1007/s13280-023-01832-5

Schütze, M., Gatz, P., Gilfedder, B., and Biester, H. (2021). Why productive lakes are larger mercury sedimentary sinks than oligotrophic brown water lakes. *Limnol. Oceanogr.* 66 (4), 1316–1332. doi:10.1002/lno.11684

Setyaningsih, C. A., Biagioni, S., Saad, A., Achnopha, Y., Sabiham, S., and Behling, H. (2018). The effect of volcanism on submontane rainforest vegetation composition: paleoecological evidence from Danau Njalau, Sumatra (Indonesia). *Holocene* 28 (2), 293–307. doi:10.1177/0959683617721329

Slemr, F., and Scheel, H. E. (1998). Trends in atmospheric mercury concentrations at the summit of the Wank mountain, Southern Germany. *Atmos. Environ.* 32 (5), 845–853. doi:10.1016/S1352-2310(97)00131-3

Smithsonian Institution (2020). *Global volcanism program*. Washington: National Museum of Natural History. doi:10.5860/choice.45-6183

Stevenson, J., and Haberle, S. G. (2005). Palaeoworks Technical Papers 5: macro Charcoal Analysis: a Modified Technique Used by the Department of Archaeology and Natural History. Technical Papers.

Swain, E. B., Engstrom, D. R., Brigham, M. E., Henning, T. A., and Brezonik, P. L. (1992). Increasing rates of atmospheric mercury deposition in midcontinental North America. *Science* 257 (5071), 784–787. doi:10.1126/science.257.5071.784

Thomas, Z. A., Mooney, S., Cadd, H., Baker, A., Turney, C., Schneider, L., et al. (2022). Late Holocene climate anomaly concurrent with fire activity and ecosystem shifts in the eastern Australian Highlands. *Sci. Total Environ.* 802, 149542. doi:10.1016/j.scitotenv.2021.149542

Turu, V., Carrasco, R. M., López-Sáez, J. A., Pontevedra-Pombal, X., Pedraza, J., Luelmo-Lautenschlaeger, R., et al. (2021). Palaeoenvironmental changes in the Iberian central system during the Late-glacial and Holocene as inferred from geochemical data: A case study of the Navamuño depression in western Spain. *Catena* 207, 105689. doi:10.1016/j.catena.2021.105689

Van Den Bergh, G. D., Li, B., Brumm, A., Grün, R., Yurnaldi, D., Moore, M. W., et al. (2016). Earliest hominin occupation of Sulawesi, Indonesia. *Nature* 529 (7585), 208–211. doi:10.1038/nature16448

Van der Ent, A., Baker, A., van Balgooy, M., and Tjoa, A. (2013). Ultramafic nickel laterites in Indonesia (Sulawesi, Halmahera): mining, nickel hyperaccumulators and opportunities for phytomining. *J. Geochem. Explor.* 128, 72–79. doi:10.1016/j.gexplo.2013.01.009

Walsh, R. P. D., and Lawler, D. M. (1981). Rainfall seasonality: description, spatial patterns and change through time. *Weather* 36 (7), 201–208. doi:10.1002/j.1477-8696.1981.tb05400.x

Wang, F., Qian, N., and Zhan, Y. (1995). *Pollen flora of China*. Beijin, China: Science China Press.

Wang, Q., Li, Y., and Wang, Y. (2011). Optimizing the weight loss-on-ignition methodology to quantify organic and carbonate carbon of sediments from diverse sources. *Environ. Monit. Assess.* 174, 241–257. doi:10.1007/s10661-010-1454-z

Wang, X., Bao, Z., Lin, C. J., Yuan, W., and Feng, X. (2016). Assessment of Global Mercury Deposition through Litterfall. *Environ. Sci. Technol.* 50 (16), 8548–8557. doi:10.1021/acs.est.5b06351

Whitten, A. J., Mustafa, M., and Henderson, G. S. (1988). *The ecology of Sulawesi*. Indonesia: Gadjah Mada University Press.

Wicaksono, S. A., Russell, J. M., and Bijaksana, S. (2015). Compound-specific carbon isotope records of vegetation and hydrologic change in central Sulawesi, Indonesia, since 53,000 yr BP. *Palaeogeogr. Palaeoclimatol. Palaeoecol.* 430, 47–56. doi:10.1016/j.palaeo.2015.04.016

Wilcken, K. M., Hotchkis, M., Levchenko, V., Fink, D., Hauser, T., and Kitchen, R. (2015). From carbon to actinides: A new universal 1MV accelerator mass spectrometer at ANSTO. *Nucl. Instrum. Methods Phys. Res. Sect. B Beam Interact. Mater. Atoms* 361, 133–138. doi:10.1016/j.nimb.2015.04.054

Yagasaki, Y., Mulder, J., and Okazaki, M. (2006). The role of soil organic matter and short-range ordered aluminosilicates in controlling the activity of aluminum in soil solutions of volcanic ash soils. *Geoderma* 137 (1–2), 40–57. doi:10.1016/j.geoderma.2006.07.001

Zhang, H., Holmes, C., and Wu, S. (2016). Impacts of changes in climate, land use and land cover on atmospheric mercury. *Atmos. Environ.* 141, 230–244. doi:10.1016/j.atmosenv.2016.06.056

Zhang, H., Nizzetto, L., Feng, X., Borgå, K., Sommar, J., Fu, X., et al. (2019). Assessing Air-surface exchange and fate of mercury in a subtropical forest using a novel passive exchangemeter device. *Environ. Sci. Technol.* 53 (9), 4869–4879. doi:10.1021/acs.est.8b06343

Zheng, W., Obrist, D., Weis, D., and Bergquist, B. A. (2016). Mercury isotope compositions across North American forests: mercury Isotopes Across U.S. Forests. *Glob. Biogeochem. cycles* 30 (10), 1475–1492. doi:10.1002/2015GB005323

Zhu, W., Lin, C. J., Wang, X., Sommar, J., Fu, X., and Feng, X. (2016). Global observations and modeling of atmosphere–surface exchange of elemental mercury: a critical review. *Atmos. Chem. Phys.* 16 (7), 4451–4480. doi:10.5194/acp-16-4451-2016